ČESKÉ VYSOKÉ UČENÍ TECHNICKÉ

FAKULTA STROJNÍ

DEPARTMENT OF AUTOMOTIVE, COMBUSTION ENGINE AND RAILWAY ENGINEERING

Simulation of Transmission Error Using FEM

Simulace chyby převodu pomocí MKP

Diplomová práce

YUJIN KIM

Study program:	Master of Automotive Engineering
Thesis supervisor:	Ing. Lukáš Kazda

MASTER'S THESIS ASSIGNMENT

I. Personal and study details

Student's name: **Kim Yujin** Personal ID number: **472138**

Faculty / Institute: **Faculty of Mechanical Engineering**

Department / Institute: **Department of Automotive, Combustion Engine and Railway Engineering**

Study program: **Master of Automotive Engineering**

Branch of study: **Advanced Powertrains**

II. Master's thesis details

Master's thesis title in English:

Simulation of transmission error using FEM

Master's thesis title in Czech:

Simulace chyby převodu pomocí MKP

Guidelines:

Make a research about transmission error.
Build a FEM model of a single stage gearbox and simulate static and dynamic transmission error. Start with a simple model and then gradually improve it to make it more complex.
Take part in experiments on test stand and compare obtained results with FEM simulation.

Bibliography / sources:

Name and workplace of master's thesis supervisor:

Ing. Lukáš Kazda, Department of Automotive, Combustion Engine and Railway Engineering, FME

Name and workplace of second master's thesis supervisor or consultant:

Date of master's thesis assignment: **09.03.2020** Deadline for master's thesis submission: **14.08.2020**

Assignment valid until: _____

Ing. Lukáš Kazda	doc. Ing. Oldřich Vítek, Ph.D.	prof. Ing. Michael Valášek, DrSc.
Supervisor's signature	Head of department's signature	Dean's signature

III. Assignment receipt

The student acknowledges that the master's thesis is an individual work. The student must produce her thesis without the assistance of others, with the exception of provided consultations. Within the master's thesis, the author must state the names of consultants and include a list of references.

Date of assignment receipt _____ Student's signature _____

© ČVUT v Praze, Design: ČVUT v Praze, VIC

ACKNOWLEDGEMENTS

I would like to express sincere appreciation to Ing. Lukáš Kazda for guiding this thesis overall in spite of his heavy schedule. As a supervisor, he has gladly given a number of advice and supports.

I feel grateful for the opportunity to be educated at Czech Technical University in Prague, by excellent professors and lecturers.

Thanks to my partner Ondřej Hula. I cannot imagine I can finish my study without his encouragement and patience.

Above all, I appreciate all supports and trust of my family toward me as their little daughter far from home. It always has brought me a great motive to keep going with my study and career.

Summary

Topics of the master thesis:
1. Research on transmission error
2. Finite element analysis of model by stages
3. Result comparison with experiments on test stand

Master student: Bc. Yujin Kim

Thesis supervisor: Ing. Lukáš Kazda

Goal of Research

This thesis contributes to a better understanding and an effective approach to analyze transmission error by using the finite element method on Abaqus. By the means of changing the main attributes of the gear model, we may expect the critical factor on transmission error and its impact on the comprehensive system.

Thus, it contains three parts to deliver the results. The first part is to acknowledge the concept of the transmission error and the effect of different variables on it.

The second is to execute the finite element analysis. The modeling is done from the basic coupling of the spur gear system and that of the helical gear system. Furthermore, complex coupling analyses of the transmission error based on the real model are performed. Finite element analysis program, Abaqus is introduced and data processing of it is conducted by NI DIAdem.

Lastly, this research will be compared with the result of the experimental test stand to discuss the effectiveness of the finite element method.

Keywords

Transmission error, gear pairs, finite element analysis, finite element method, Abaqus simulation, dynamic/explicit analysis, mesh elements, boundary condition, gearbox test stand

Statement of Declaration

I hereby declare that my master thesis work “Research on transmission error”, “Finite element analysis of model by stages”, “Result comparison with experiments on test stand” have been completed by myself under the guidance of the supervisor and consultants.

Yujin Kim

In Prague, on **14 – 08 – 2020**

_____

Signature

Structure

Nomenclature

a	Center distance of the uncorrected pairs of gears	[mm]
a_c	Corrected center distance	[mm]
a_w	Center distance of the pair of gears (rolling)	[mm]
α_t	Transverse pressure angle	[°]
α_{wt}	Transverse working pressure angle	[°]
α_{w}	Rolling pressure angle	[°]
α	Normal pressure angle	[°]
$\overline{AB}$	Length of the line of action	[mm]
β	Helix angle	[°]
c_d	Dilatational wave speed	[mm/s]
$d_{a1,2}$	Addendum circle diameter of input and output gear	[mm]
$d_{\mathrm{b}1,2}$	Base circle diameter of input and output gear	[mm]
$d_{f1,2}$	Dedendum circle diameter of input and output gear	[mm]
$d_{\mathrm{w}1,2}$	Rolling circle diameter of input and output gear	[mm]
$d_{1,2}$	Pitch circle diameter of input and output gear	[mm]
$E_{1,2}$	Young's Modulus of input and output gear	[MPa]
$e_{1,2}$	Circular width of tooth space of input and output gear	[mm]
F_t	frictional force	[N]
GMF	Gear mesh frequency	[Hz]
$h_{a1,2}$	Height of addendum of input and output gear	[mm]
$h_{f1,2}$	Height of dedendum of input and output gear	[mm]
$h_{at1,2}$	Height of addendum without correction of input and output gear	[mm]
$h_{1,2}$	Total height of teeth of input and output gear	[mm]
h_a^*	Addendum coefficient	[-]
h_f^*	Dedendum coefficient	[-]
i	Gear ratio	[-]
l_{min}	Smallest element dimension	[mm]
l_0	Amount of critical elastic sliding	[-]
$L_{1,2}$	Length of arc of input and output gear	[mm]
$m_{1,2}$	Module of input and output gear	[mm]
N	Normal force	[N]
p	Circular pitch	[mm]
p_b	Base circular pitch	[mm]
p_w	Circular pitch on the rolling circle	[mm]
ppr	Pulse per revolution	[ppr]
$r_{1,2}$	Pitch radius of input and output gear	[mm]
$r_{bo1,2}$	Bore radius of input and output gear	[mm]
$r_{c1,2}$	Radius of input and output shaft on clutch side	[mm]
$r_{s1,2}$	Radius of input and output shaft on sensor side	[mm]
$RPM_{1,2}$	Angular velocity of input and output gear	[rpm]
S	Slip	[-]
$s_{1,2}$	Circular thickness of tooth of input and output gear	[mm]

t	Time	[s]
TE	Transmission error	[mm]
$v_{bo1,2}$	Velocity on bore of input and output gear	[mm/s]
$v_{c1,2}$	Velocity of input and output shaft on clutch side	[mm/s]
$v_{s1,2}$	Velocity of input and output shaft on sensor side	[mm/s]
$w_{1,2}$	Base tangent length (checking distance)	[mm]
$x_{1,2}$	Profile shift factor	[-]
y	Center distance modification coefficient	[-]
Δy	Basic rack tooth profile displacement	[mm]
$z_{1,2}$	Number of teeth of input and output gear	[-]
$z'_{1,2}$	Number of teeth corresponding to the base tangent length	[-]
ε_α	Contact ratio	[-]
Δt	Time increment size	[s]
λ	Lame's modulus	[MPa]
μ_s	Shear modulus	[MPa]
$\nu_{1,2}$	Poisson's ratio of input and output gear	[-]
μ	Friction coefficient	[-]
$\theta_{1,2}$	Rotation angle of input and output gear or shaft	[rad]
$\rho_{1,2}$	Density of material of input and output gear	$[ton/mm^3]$

1. Introduction

1.1. Background

Gear is one of the great human inventions and used in an enormous range of industries, including automobiles and robotics. Following advancing modern technology and its new development, the gear part has been researched and modified. The major purpose of a gear mechanism is to transmit the rotation and torque between different axes. It is an effective and compact power transmission element. Nevertheless, during the operation, the difference by deformation occurs between the actual position of the output gear and the theoretical position where the part would place if the gear were perfectly conjugated. This is defined as a so-called transmission error.

In keeping with the current trend towards high mechanical efficiency, the pursuit of compact and lightweight transmission systems causes an increasing amount of elastic deformation of the gears. For this reason, dynamic analysis is more and more important to meet the requirement of contemporary technology. The study of gear dynamics is not a new concept and it has been investigated over a few decades. Even though a lot of related works have been carried, there is still scope to investigate certain areas that were not well discovered before. In the past, the limit on computation access was an obstacle to certain methods. And as a result, numerical methods were widespread to understand the dynamic behavior of gears. A recent development in computer software has opened innovative approaches to gear analysis. In order to examine and predict the responses of gears, computational analysis becomes more and more essential including the finite element method.

1.2. Definition of Transmission Error

The transmission error (TE for brevity) is a difference between the theoretical rotation of a gear system and the real rotation of a system. There are multiple reasons that this phenomenon occurs. It might be caused on account of deflectable parts and also the errors which are inherent in gears themselves. In the long run, the wears on gears produce unexpected and random TE by poorly manufactured gears or by long term performance.

The static transmission error mainly depends on inherent errors in the gear or the transmission design. It can be classified into three factors, which are represented by the gear profile error, the machining error, and the assembly error.

The gear profile geometry stage has been decided during the development including tooth macro geometry and micro geometry. Most of the gear tooth geometry, such as the addendum, dedendum diameters, and thickness of the tooth, is influenced by the macro design. Micro geometry design includes small modifications of the gear teeth in microscales such as crowning and relief. These designed profiles may not be optimized enough to have optimal contact patterns for the gear pair under different loads and speeds. Transmission error minimization is highly dependent on this stage and achieving the target design criteria is a critical job.

The gear machining error is closely connected to the gear profile shape and it has a great effect on the transmission as well. Under poor performative manufacturing environment, the gear

tooth contains defects resulting in the output gear being ahead or after of its theoretical position. This transmission error is positive when a small particle or a burr presents on the surface. It can be also negative when teeth deflect elastically under load. Due to a machining tolerance and a tool accuracy, a certain error exists between the actual tooth surface and theoretical tooth surface. The actual surface contains comprehensive errors including profile error ($f_{\mathrm{H}\alpha}, f_{f\alpha}$), helix error ($f_{\mathrm{H}\beta}, f_{f\beta}$), and pitch error ($f_{pt}$). Figure 1[1] below shows how the final surface can look like with each error after being machined.

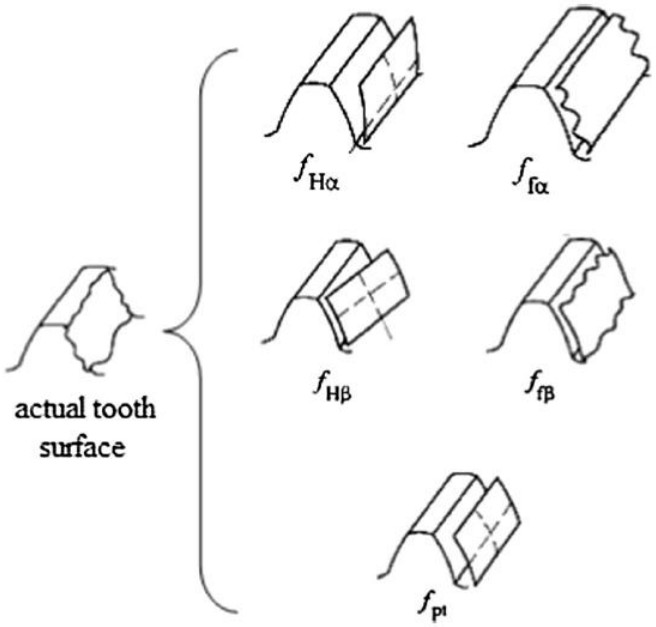

Figure 1. Actual tooth surface with machining error [1]

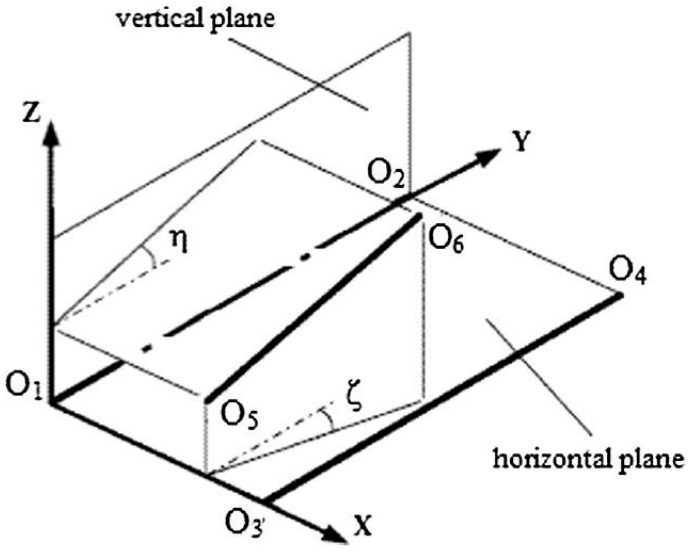

Figure 2. Assembly error [1]

In the assembly process of a gearbox, assembly error occurs at all times. Figure 2[1] above shows classified assembly error with respect to the direction. The deviation of the axis causes

the gears to be misaligned by creating angles in the vertical plane(η) and angles in the horizontal plane(ξ). This error has a great influence on the transmission error of the total gear system in turn.

Furthermore, the driving condition with high speed should be considered. In the case of perfect involutes and an infinite stiffness, the rotation of the output gear would be a function of gear ratio. It means that the constant input speed results in the constant output speed. In reality, however, the stress is produced when the gears have meshed together, the deformation such as tooth bending and tilting takes place. This dynamic excitation along the mesh causes the displacement among gears. The spatial difference in this high-speed operation is called dynamic transmission error.

Before elaborate on the further calculation procedure which is the data processing method in this study, a simple mathematic equation is introduced. In Figure 3, a simplification of a pair of gears is drawn. Two externally tangent circles represent pitch diameters of input and output gear. When the two mechanical parts are ideally rotating along the mesh line, they must have the same arc length, which is indicated by green color arcs. This can be expressed by a simple equation.

$$L_{1,\,ideal} = L_{2,\,ideal} \tag{1}$$

$$(L = length\ of\ arc\ on\ pitch\ circle)$$

However, due to the transmission error, the real arc lengths can differ from each other.

$$L_{1,real} \neq L_{2,\,real} \tag{2}$$

Thus, the TE of a gear pair can be expressed by the measured angle of rotation. This can be shown as the following formula for a linear discrepancy.

$$TE = L_{2,real} - L_{1,real} = \theta_2 r_2 - \theta_1 r_1 \tag{3}$$

θ_1 and θ_2 denote the rotation angle of input and output gear. r_1 and r_2 are the pitch radius of input and output gear respectively. As mentioned, this equation comes from the simple idea that the lengths of the arcs of tangent circles are equal.

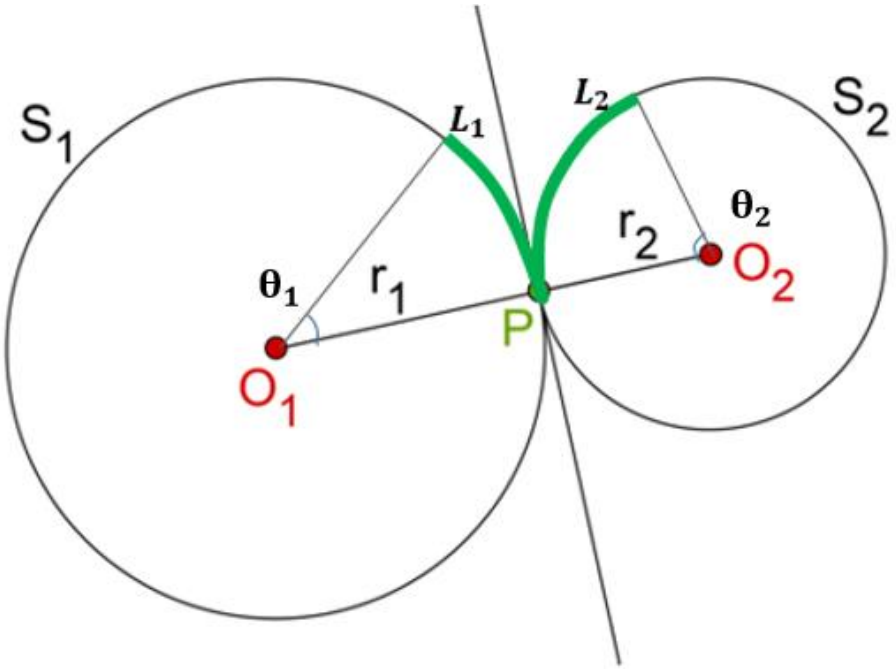

Figure 3. Externally tangent circles

1.3. Review of Previous Research

Several types of researches regarding transmission error have been carried out by various methods. One of the remarkable work by Lin, T. and He, Z. [1] has used an analytical method for coupled transmission error of a helical gear system in a marine gearbox. The goal of this study was to control the vibration and noise of the gear system. The authors presented equations as a mathematical tooth profile model of a helical gear with profile error and helix shape error. Based on the equations of the derived tooth profile with error, MATLAB code was developed to generate 3-D coordinates of discrete points on the tooth surface of helical gears. The machining error has been expressed as a form of two angle deviations as shown before in Figure 2. Then, all synthesized factors have adapted to the finite element analysis model for the calculation of the mathematical model and the comprehensive influence of such factors on the transmission error of the gear transmission system has been studied. For instance, the following plots in Figure 4 express the impact of assembly error on the vertical and horizontal planes on TE.

Not only the static transmission error but also the dynamic transmission error has been handled. The bending, torsional, and axial discrete dynamic model of a marine gearbox is created with a lumped mass method based on the static transmission error. Two input gears and one output gear with the time-varying stiffness and the damping are newly established. It has evaluated peak-to-peak value of dynamic transmission error while input torques are the same and input speeds are changing from 50rpm to 2000rpm with 50rpm intervals as shown in Figure 5 below. The outer envelope lines of the dynamic transmission errors of gear pairs

are used to represent the TE of the whole system.

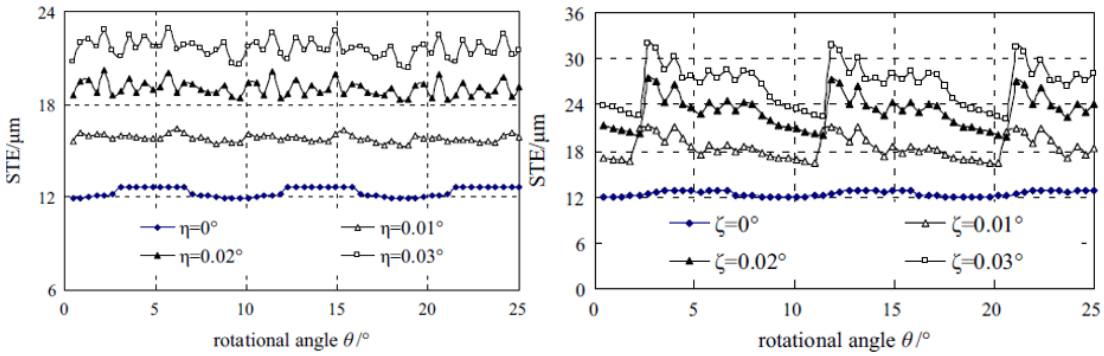

Figure 4. Static transmission error with assembly error [1]

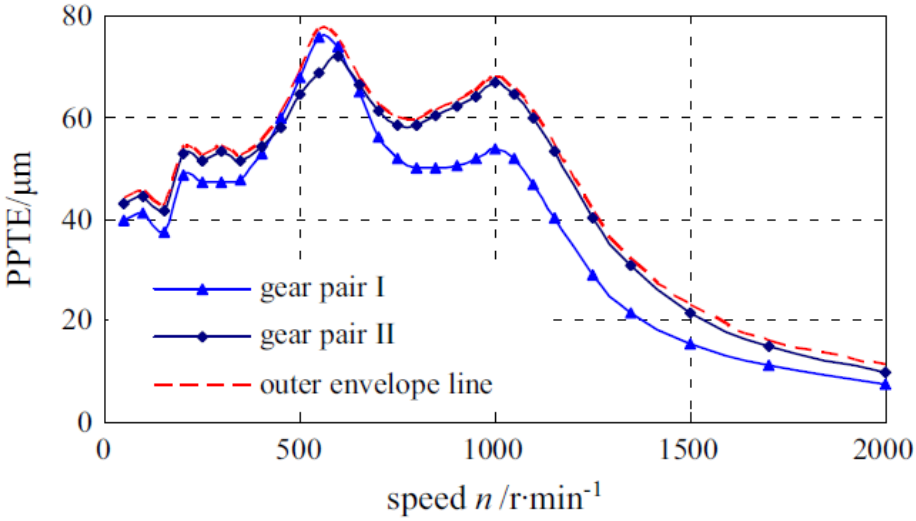

Figure 5. The peak-to-peak of TE of helical gear pair [1]

Other research [2] has shown how the general finite element method can be applied to study dynamic behavior in the case of an actual gearbox. The transmission model with two pairs of spur gears is simplified to obtain the equations about its contact information. With the values from the finite element method, the equations are solved to obtain a distribution of dynamic contact load, contact stress, and strain on one node. Korde, A. and Mahendraker, V. [3] have chosen the finite element method to compare their mathematical work to FE as well. The FEM model is created to verify their mathematical model of the gear train and update the model. The dynamic transmission error difference by various gear profile modifications has been checked. It is furtherly discussed for gear noise problem and optimization of gear microgeometry within an acceptable range which is feasible for manufacturing.

One thesis [4] has undertaken a comparison among dynamic transmission errors of spur gears with variables using FEM. Abaqus program has been used for 2-D spur gear analysis as shown in Figure 6. It also contributes to understanding the level of accuracy entailed by such an analysis and how that is related to the many parameters such as parameters for the contact algorithm, the convergence tolerance, and so on. With several variations of the input parameters or the gear design, it has shown the effect of each variable on the transmission

error. One example is shown in Figure 7, which is an effect of varying torques on dynamic transmission error. The obtained results are used to study the effect of intentional tooth profile modifications on the transmission error, involving the development of an optimization algorithm to design the tooth modifications.

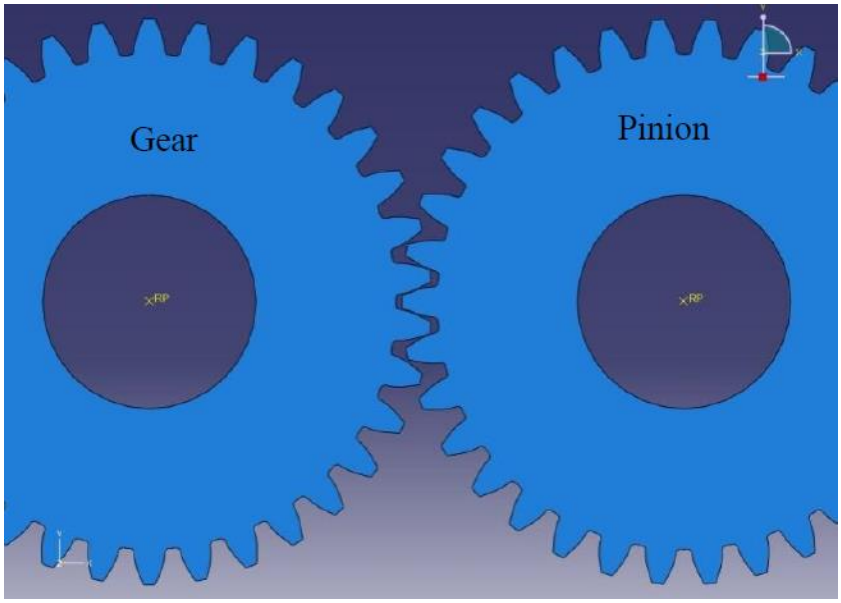

Figure 6. 2-D spur gear model [4]

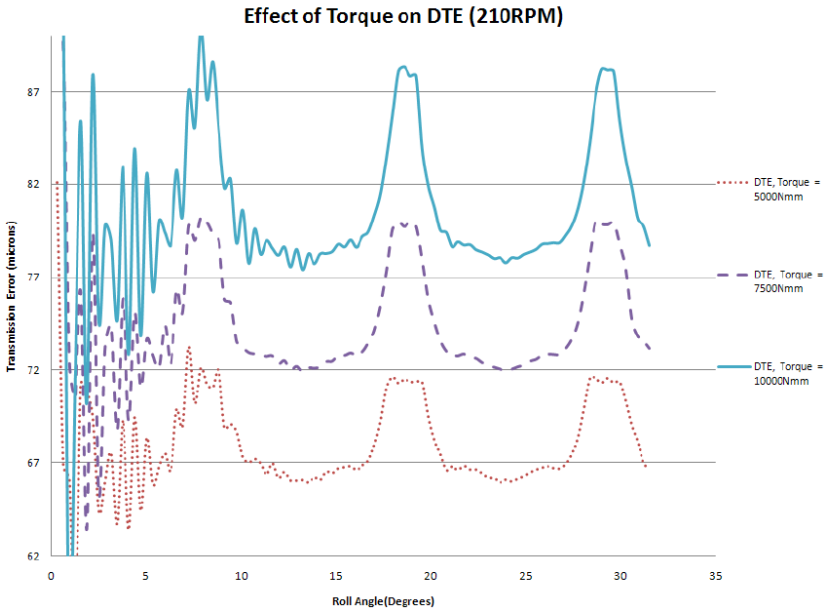

Figure 7. Dynamic transmission error for varying torques [4]

In another manner [5], multibody modeling is introduced to reduce the computational expense of 3D finite element analysis. A multibody system with paired spur gears and helical gears are modeled that are taking into account the gradually varying operating conditions such as load and speed. In one study by SAE [6], multibody dynamics are adapted based on the test rig to compare the TE with ideal and real gear models as shown in Figure 8. To achieve a

reasonable degree of correlation between experiment and simulation, adequate representation of the test rig such as bearing, shafts, and clutches are incorporated in the model. Focusing on the gear profile shapes, the frequency spectrum of simulated transmission error for ideal and real flank shapes have been compared under the same load condition. The result in Figure 9 shows the distinction between real and ideal profile becomes extremely obvious when comparing peak-to-peak TE in the frequency domain. It has implied that the quality of simulations is highly dependent on the ability to specify "close to reality" profile shapes and the structure of the tested model.

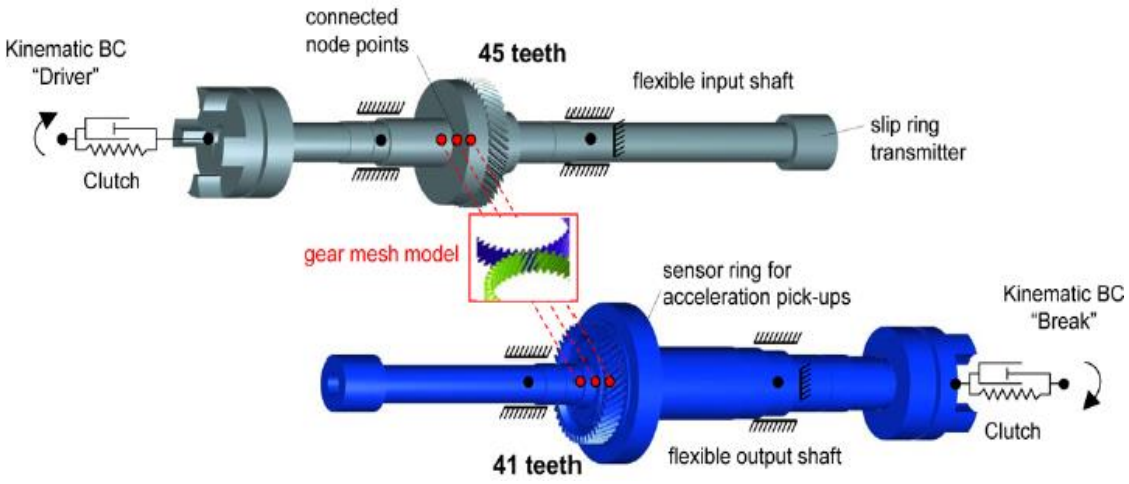

Figure 8. Multibody dynamic model of test rig [6]

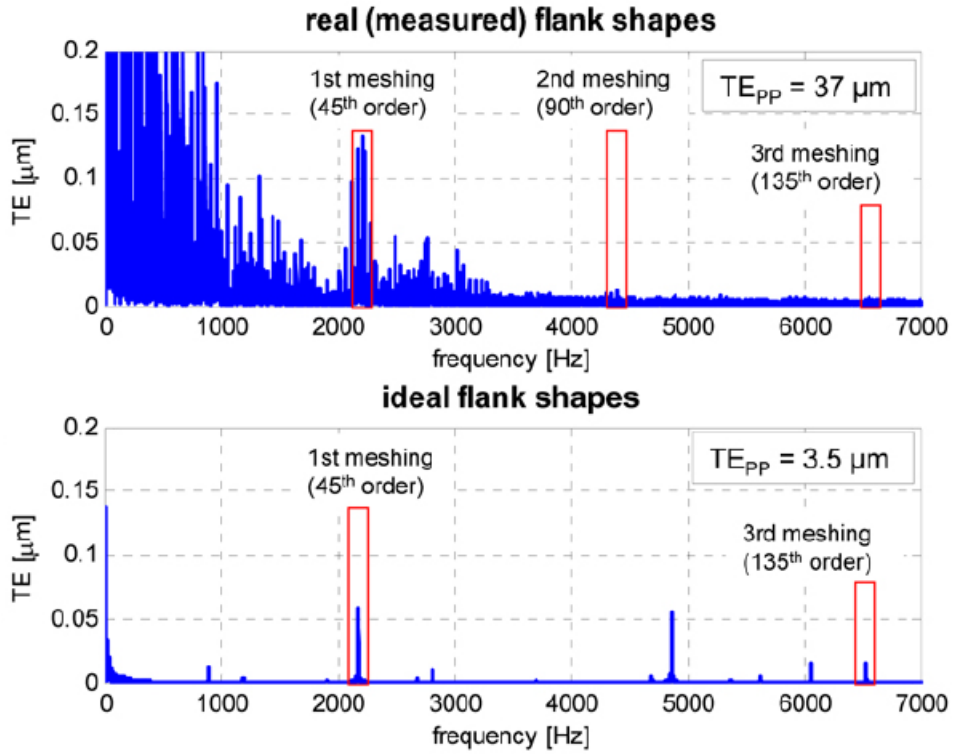

Figure 9. Spectrum of simulated TE for ideal and real flank shapes [6]

As an empirical method, transmission error for heavy-duty gearbox has been measured by researchers of Brno University of Technology [7]. A measuring loop has been assembled from two gearboxes and the rotary encoders. The main purpose was to evaluate the impact of the different transmitted torque under the same input velocity. At the input speed of 50rpm, the torque range has changed from 600 to 2400Nm. For data processing, a script in MATLAB software was built to calculate TE and it was used as a benchmark for vibration prediction.

These studies give a very fine overview and introduction into the area of transmission error in gears. TE has been revealed under various conditions such as tooth profile difference, speed, and torque. Different methods including analytical and empirical ways are used to obtain the results. Despite numerous perspectives about transmission error, they mainly focus on the static error on the transmission which is affected by the dynamic characteristics of parts while being driven at high speed. Also, there are many simplifications in analytical ways when finding total transmission error by summing up each of the transmission errors followed by different factors. Total transmission error cannot be decided only by linearly summing up all of these matters because the effect of interaction among each characteristic error on dynamic excitation is barely considered. A number of studies with one pair of gears are not able to describe the influence of other components. In automotive application, it has been proven that this error is mutually expressed in the system consisting of gears, bearings, and shafts. For decades, there have been several experiments conducted to represent the influence of the dynamic transmission error. Following the structure of the test stand which will be further compared with the result by FEA, the model of this research is carried out under certain conditions with load and speed.

1.4. Required Constraints and Assumptions

This research is about the simulation of transmission error based on the finite element analysis. The topic has been widely dealt with by many approaches, such as the 1-D torsional models and engaged line models. This simple 1-D model, as well as the models which reduce gear interaction, does not resolve the contact of the mating mesh in detail. The main advantage of these assumptions on the 1-D model is to moderate computational effort. However, some drawbacks following such assumptions must be counted. Firstly, the irregularity of the load distribution by the gear misalignment is not detected. Secondly, the meshing stiffness used as an input is derived for an ideal condition that may not correspond to the actual dynamic motion of the meshing gears. Third, actual load distribution and contacts along the flank remain undetected. Hence, the 3-D design is preferred to it to consider appropriate input values for overall gear stiffness on the rolling angle.

Behind these, some assumptions are still existent in this thesis. As the parts are designed elaborately by the computer-aided design program, it is inevitable to count out several factors causing errors that have been mentioned above, such as assembly error and manufacture error. Typical gear optimization such as relief or crowning is not included. Also, the deformation which is dependent on temperature remains unknown. This may suppose that meshing stiffness used in the simulation is under ideal conditions and may not correspond to the practical dynamic motion of the paired gear wheels.

1.5. Finite Element Software – Abaqus/Explicit

In recent years, there have been remarkable developments in direct computer-aided engineering. As a result, engineers can undertake a wide range of design, analysis, and modeling in their research fields. One of the aims of this study is to establish a simple FEM procedure that is capable of the modeling gear system, simulating under its respective operating conditions.

In this study, the main work is done by Abaqus. One of the modules inside the Abaqus, Abaqus/Explicit, provides finite element analysis with various simulation tools for brief transient dynamic events. It is applicable to the simulation where high-speed, non-linear, and transient response dominates the solution. As the topic is mainly about the simulation of the dynamic transmission error on the gears functioning at high speed, this program is selected as an appropriate one. Abaqus has a workflow in the simulator which can be found in Figure 10. The following analysis flow diagram is adapted for the transmission error simulation. Each step is dealt with in more detail later on.

1.6. Data Processing Software – NI DIAdem

The raw data from the Abaqus is not enough to know wanted information about transmission error by intuition. As the goal of the study is to know the transmission error by the finite element method and to compare it with the transmission error from the real test stand, additional data processing is required. NI DIAdem is used to accelerate the post-processing of measurement data. It is the tool that can optimize the large data set and automate the repetition in the calculation. This software is used to manage the data on each analysis.

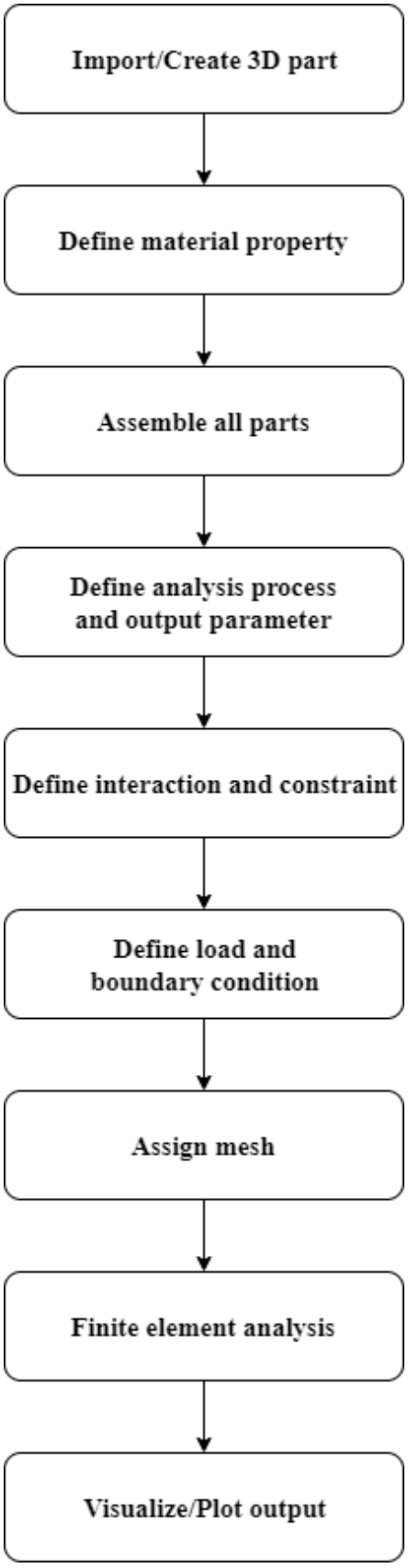

Figure 10. Abaqus work flow

2. Experimental Research

2.1. Background

The goal of this thesis is to compare the transmission error from the test rig and the FEM. For that, the experimental test stand must be first mentioned before discussing all the analysis process and before the comparison of results. This chapter explains the setup of the rig and its data acquisition. The given data of transmission error are plotted and analyzed.

2.2. Experimental Setup

The configuration of the test bench is in Figure 11[8] below. It mainly consists of six parts. From the left-hand side to the right-hand side, in numerical order, speed sensors, measured gear set, clutch, grooving for applied load, torque sensor, and another gear set are located. On the end of the input gear shaft, an electric motor places and it controls the rotation instead of an engine. To apply the required torque on the shaft, a bar that can join on the groove can be fitted and extra weights are added on the end. The size of torque can be simply calculated by multiplication of the bar length and the weight.

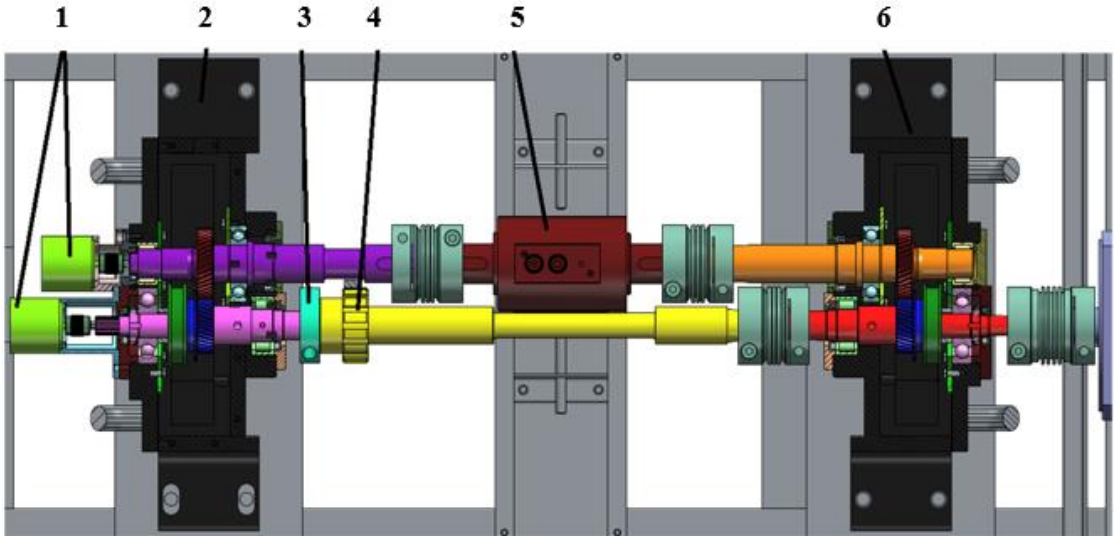

Figure 11. Test rig configuration [8]

For sensing the speed of each shaft, incremental rotary encoders have been used to collect the rotational period of the shafts and to send the data to the computer for display and post-processing. An encoder is an electrical and mechanical device that converts rotary displacement into pulse signals. The most popular type of encoder is an optical encoder. This consists of a light source, a light receiver, and a disk. This disk has an optical pattern that repeats opaque and transparent sectors and this is electronically decoded to generate position information by rotation. The key to getting the electronic information is up to the light emitter and receiver. When the opaque sector blocks the light which emits onto the receiver and when the transparent sector lets the emitted light reach the receiver, it generates a pulse signal output. A pulse for each incremental step in the encoder is generated and these characteristics enable high resolution. Commonly the encoders have three outputs. Two outputs have the same pulse per

revolution rate with 90 degrees out of phase. This allows the identification of the direction of rotation. The other output has a reference pulse or so-called, zero signal, generating once per revolution to set the reference position.

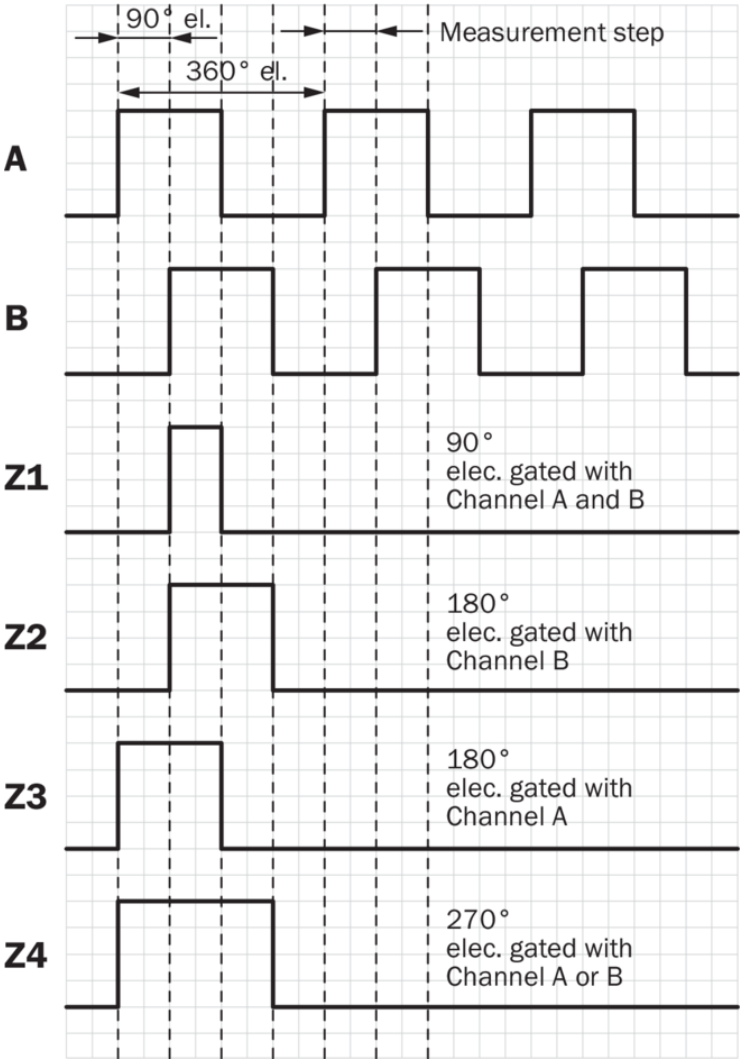

Figure 12. Encoder pulse diagram [9]

The incremental encoder which is utilized in the test rig, SICK DFS60, provides transistor-transistor logic (TTL) interface which is in ranges between 0-5V. This model has a differential conductor pair for the logic outputs as shown in Figure 12 [9]. Based on two outputs A and B which lie with 90 degrees of phase difference, logically gated four other outputs are expressed. When the long cable lengths are connected with the encoders, random electromagnetic fields or currents from outside induce undesired voltages, which cause noise. With the differential pair of signals, this noise can be eliminated by summing up the voltage of each pair and retain the original voltage. These characteristics allow high-frequency response capability and noise immunity. This employed model (type DFS60B-S1PL10000) creates 10000 samples per revolution, which means that it detects every 0.036° of the rotation. Afterward, this should be counted during the FEM model creation.

2.3. Data Acquisition and Processing

Despite the usage of high performing encoders, filtering is essential to remove unwanted noise. In this test stand, a lot of fluctuation on the actual speed due to the noise and runout of gears or other components can corrupt the encoder signal. To eliminate this undesired behavior, filtering is essential. In this case, a Bessel filter is selected for signal processing. The filter is optimized to provide a constant group delay in the filter passband while sacrificing sharpness in the magnitude response. It may reduce the unexpected noise from the data.

Besides, the fast Fourier transformation (FFT) method is used to analyze the transmission error. When the original signals are generated in electric devices, those are concerning the real-time base. These output signals may be frequently misunderstood that they are not periodic and arbitrary in the time domain. However, the signals are, in fact, a combination of sinusoidal oscillations. By using FFT combined oscillations can be converted into individual spectral components, which indicates each frequency information inside the given signals.

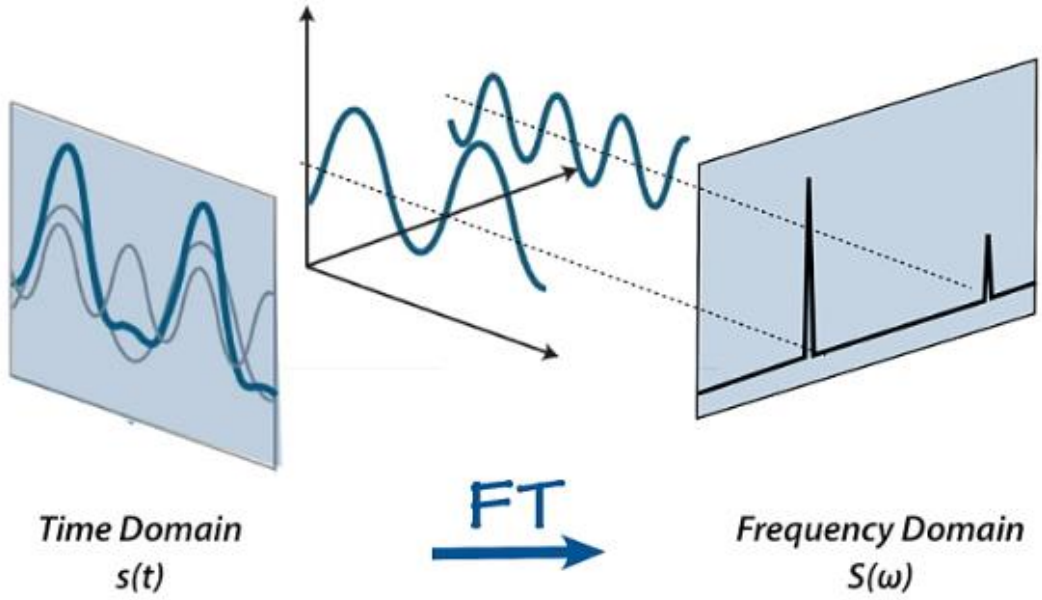

Figure 13. Fourier transformation [10]

For example in Figure 13 above [10], the time domain signal contains two different single sinusoidal oscillations at distinct frequencies with their own phase and amplitude. This frequency domain can give a clue about elements inside the transmission error. In this study, the frequency domain is expected to inform the gear mesh frequency, which is the characteristic of each gear assembly. Gear mesh frequency can be calculated using the following equation, where z is the number of gear teeth and RPM is the rotating speed of the gear. The formula can be used not only on the input gear but also on the output gear. Numbers 1 and 2 are applied to driving input and driven output gear respectively.

Gear mesh frequency $$GMF = z_1 \cdot \frac{RPM_1}{60} = z_2 \cdot \frac{RPM_2}{60} \quad [Hz] \qquad 4$$

2.4. Transmission Error

The experiment has been conducted with various input speed. For dynamic analysis, changing the range of velocity from 250 rpm to 5000rpm with the same torque, the same tests are undertaken. After data acquisition from encoders, the transmission error is calculated and its value is filtered to reduce the noise effect by the runout of components.

Figures 14 and 15 show filtered transmission error of the test rig when input rotation rates are 130.9 rad/s (1250rpm) and 209.44 rad/s (2000rpm) with the same torque. To have a close look at the shape of the transmission error, the time band is shortened until the input gear rotates about two revolutions. There is a lot of fluctuation due to the vibration from other components in the test stand. Some peaks which do not follow the tendency can be from electric noise since it is not filtered out. The amplitude of the wave of transmission error, therefore, teeters as well. At 1250rpm, TE begins with approximately 0.01mm of amplitude and oscillates bigger and smaller. At 2000rpm, the pattern of transmission error is more ambiguous to see a certain shape due to the high vibration. Nonetheless, the amplitude value seems to be still in the ranges of -0.005mm and 0.005mm.

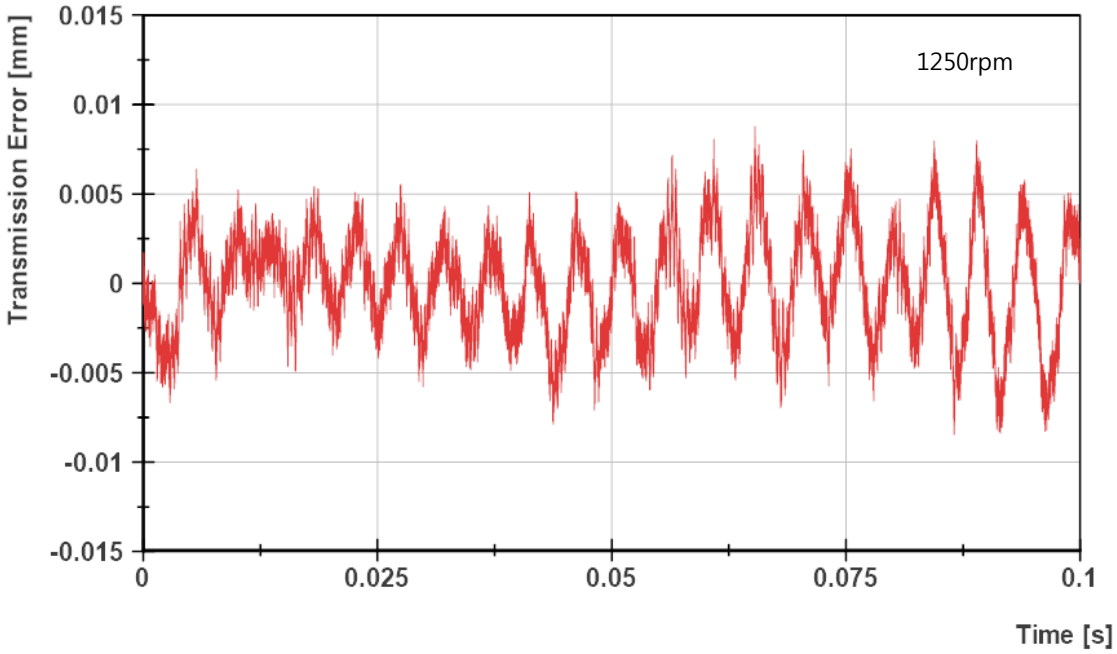

Figure 14. TE of test rig at 1250rpm

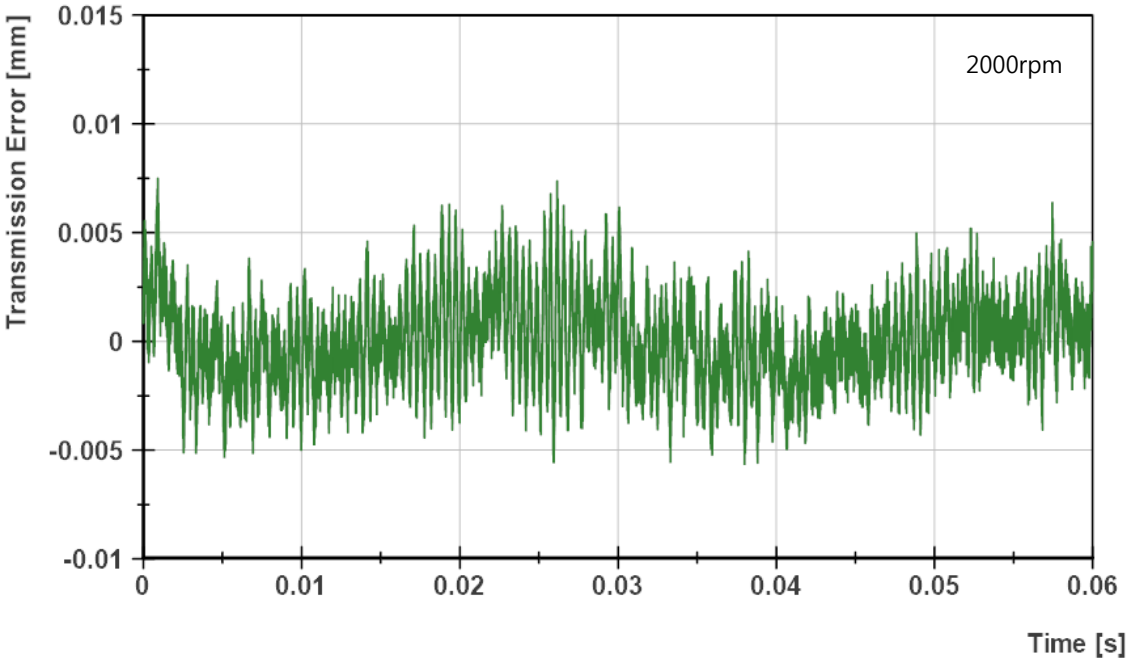

Figure 15. TE of test rig at 2000rpm

The static transmission error could be obtained as well at a low speed. Figure 16 shows the result at the input angular speed of 6.28rad/s (60rpm). A decrease of dynamic interaction among other components in the system brings the result that its amplitude of TE also has decreased to 1/5 level of the amplitude of the dynamic transmission error. Due to the instability of the electric motor at a low speed, some irregular fluctuations are generated from time to time.

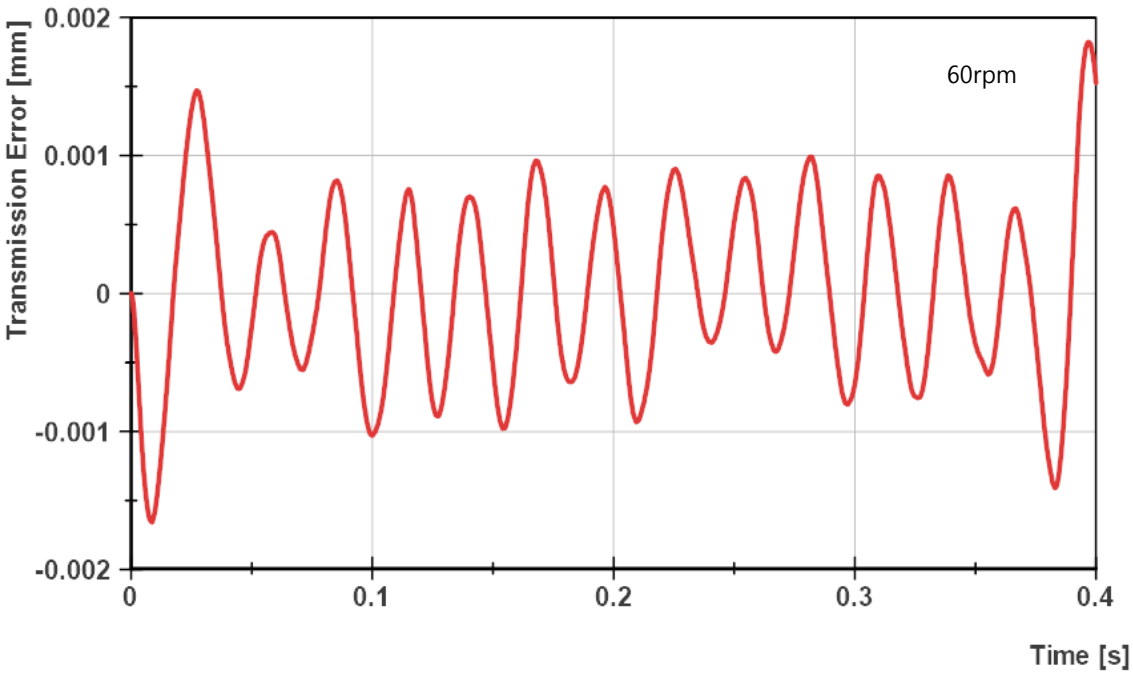

Figure 16. TE of test rig at 60rpm

As it is described in the previous chapter, the time domain signal contains different single sinusoidal oscillations. Mainly at GMFs, the signals have their phases and amplitudes. If the frequency domain is known, its original time domain can be deduced back. Thus, the frequency domain is also good to be known to characterize the curve. Especially for dynamic analysis, it is recommendable to look at the FFT result to verify the result. It would give a clue about elements inside the transmission error. To verify the ingredients inside the two given time domains, the fast Fourier transform method is used on both transmission error graphs.

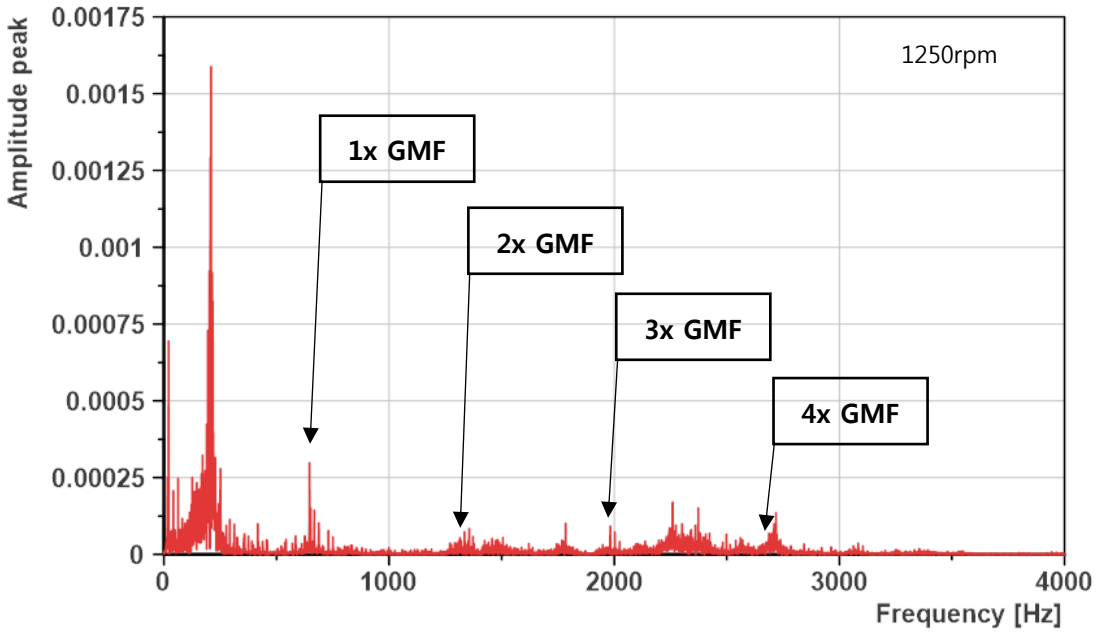

Figure 17. Amplitude peak by frequency spectrum of test rig at 1250rpm

In Figure 17, the constituent frequency of the transmission error at 1250rpm has been plotted. The frequency band is shortened because the amplitude at the high-frequency zone is trivial enough compared to the amplitude until 4000 Hz. By using Equation 4, gear mesh frequency is calculated. Based on obtained GMF with a value of 666.7Hz, integer multiplied frequencies become its second, third GMF, and so on. While the first and third meshing orders are visible, the second and fourth meshing frequency shows small magnitudes only.

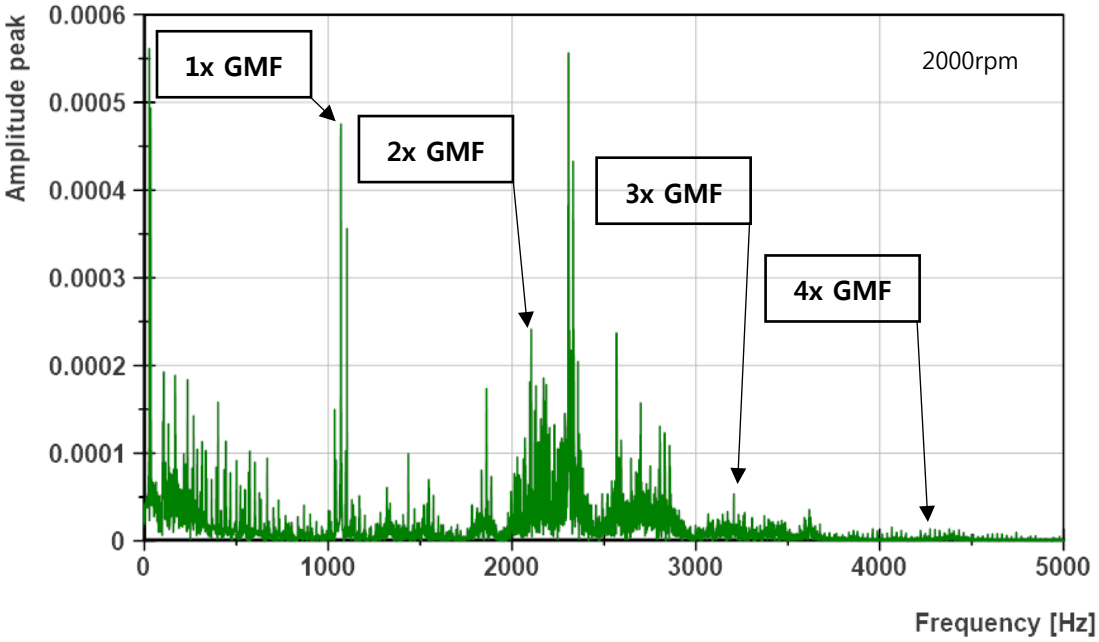

Figure 18. Amplitude peak by frequency spectrum of test rig at 2000rpm

In Figure 18, the frequency domain of transmission error at 2000rpm can be found. The frequency band is modified until 5000Hz due to the same reason as the previous case. The amplitude diminishes remarkably in the high-frequency zone. Since this frequency is far below the range of possible gear mesh excitation, the effect by it on GMF is not noticeable. The first GMF is at 1066.7Hz and the families with integer multiplications are marked on the graph.

Some peaks on the certain frequencies seem that they are typically higher than on the gear mesh frequency but still they may not be related to the geometry of the gear. It can be due to manufacturing errors on components in the test rig. Also, some of the peaks may be driven by the vibration of other parts in the drivetrain or by electric noise. According to the highest peak in both graphs, the low natural frequency of the assembly can closely locate at 200Hz. It can correspond to the rotational vibration mode constituted by the compound inertia of gears, clutches, shafts, and sensors. Between 2000Hz and 3000Hz, at both speeds contain peak amplitude that is much higher than GMF. Seemingly, some natural frequencies of the system are present in that zone. In general, it is visible that the highest amplitudes in meshing orders appear in resonance cases when the gear excitations coincide with the system's natural frequencies.

3. Methodology Using Simplified Spur Gear Model

3.1. Introduction

The analyses in this thesis go through three main stages. From the simplest spur gear model and the helical gear model which is designed based on actual gears in the experimental test rig to the complex helical gear model consisting of additional mechanical components are analyzed in sequence.

Firstly, in this chapter, the instrumental program and main procedure of analysis are introduced with a pair of basic spur gears. With this simple spur gear model, the outline of this research can be established before going any further. This helps familiarization with the approach to the higher level of modeling as well as with the efficient means to get a desirable result. Furthermore, it can prevent the research from confronting elementary misunderstanding and the following severe error. This effort of gear wheel modeling and computation is beyond the scope of the product development process. Nonetheless, it still ought to be covered to understand the fundamental knowledge of FEM via Abaqus and data acquisition which are important for the next steps. So this first chapter may be called a “Learning stage”.

Once the study about the FEM program Abaqus and data acquisition is done by the aid of the spur gear model, a pair of helical gear is created. It is better to know the new model that is closer to the final step as a groundwork to deal with a more complex model. New characteristics can be found and be modified which have not appeared in the first model. Not only the modeling and finite element method but also the basic data processing with the obtained result is introduced by the software NI DIAdem. While undertaking the analyses with different conditions and a longer period, it is possible to face unexpected problems. Dealing with problems and presenting appropriate solutions are simple to be done in this stage because the computational effort to conduct these can be overly big in the next complex model. Therefore, this second chapter may be called a “Trial and error stage”

At last, an assembly model is introduced which consists of gears and shafts. Both adapting the extra components and adding new boundary conditions and interaction between the parts are essential in this thesis on account of the dynamic behavior. As mentioned in the “Introduction” chapter, the transmission error is influenced not only by the defects on the tooth profile or the manufacturing process but also by interplays among other excitation sources such as bearing and clutches. This last chapter can be called a “Target stage” and its result will be compared to the experiment.

By going through these steps, this paper could be accessible even to the ones who are not accustomed to the finite element method or the transmission error and be supportive of the future work regarding the similar method.

3.2. Finite Element Analysis of Spur Gear

3.2.1. Part creation

First of all, the spur gears should be created as a basic step to make a finite element model of gear pair. Main parameters are given and the most often used coefficients are added for a better design of tooth profile. The values are shown in Table 1 below. These are fictive numbers that are inspired by some parameters of helical gears in the test rig.

Spur gear parameters	
Normal module ($m_{1,2}$)	1.5mm
Pressure angle (α)	17°
Number of teeth of input gear(z_1)	32
Number of teeth of output gear(z_2)	41
Addendum coefficient (h_a^*)	1
Dedendum coefficient (h_f^*)	1.25
Profile shift factor ($x_{1,2}$)	0

Table 1. Spur gear parameters

These given values are not enough to design a gear profile since even a simple gear contains many other parameters. With equations [11] on the following table, other necessary geometrical parameters can be obtained by a few calculations. As the gear profile shift factor is not considered, many of the equations can be simplified.

Gear ratio	$i = \frac{z_2}{z_1}$	5
Pitch circle diameter	$d_{1,2} = m_{1,2} \cdot z_{1,2}$	6
Base circle diameter	$d_{\mathrm{b}1,2} = d_{1,2} \cdot cos\alpha$	7
Centre distance of the uncorrected pairs of gears	$a = \frac{z_1 + z_2}{2} \cdot m = \frac{(d_1 + d_2)}{2}$	8
Rolling pressure angle	$inv\ \alpha_{\mathrm{w}} = inv\ \alpha + \frac{2 \cdot (x_1 + x_2) \cdot tg\ \alpha^{\circ}}{z_1 + z_2}$	9
Rolling circle diameter	$d_{\mathrm{w}1,2} = d_{1,2} \cdot \frac{cos\ \alpha}{cos\ \alpha_w}$	10

Centre distance of the pair of gears (rolling)	$a_w = a \cdot \frac{cos\ \alpha}{cos\ \alpha_w}$	11
Basic rack tooth profile displacement	$\Delta y = \frac{a + (x_1 + x_2) \cdot m - a_w}{m} = \frac{a_t - a_w}{m}$	12
Height of addendum	$h_{a1,2} = h_{at1,2} - \Delta y \cdot m$	13
Height of addendum without correction	$h_{at1,2} = h_a^* + x_{1,2} \cdot m$	14
Height of dedendum	$h_{f1,2} = h_f^* \cdot m - x_{1,2} \cdot m$	15
Total height	$h_{1,2} = h_{a1,2} + h_{f1,2}$	16
Addendum circle diameter	$d_{a1,2} = d_{1,2} + 2 \cdot h_{a1,2}$	17
Dedendum circle diameter	$d_{f1,2} = d_{1,2} - 2 \cdot h_{f1,2}$	18
Circlular pitch	$p = \pi \cdot m$	19
Base circular pitch	$p_b = p \cdot \frac{d_{b1,2}}{d_{1,2}} = p \cdot \frac{d_{1,2} \cdot \cos\alpha}{d_{1,2}} = p \cdot \cos\alpha$	20
Circular pitch on the rolling circle	$p_w = p \cdot \frac{\cos\alpha}{\cos\alpha_w}$	21
Circular thickness of tooth	$s_{1,2} = \frac{p}{2} + 2 \cdot x_{1,2} \cdot m \cdot tg\ \alpha$	22
Circular width of tooth space	$e_{1,2} = \frac{p}{2} - 2 \cdot x_{1,2} \cdot m \cdot tg\ \alpha$	23
Length of the line of action	$\overline{AB} = g_\alpha = \sqrt{\left(\frac{d_{a1}}{2}\right)^2 - \left(\frac{d_{b1}}{2}\right)^2} + \sqrt{\left(\frac{d_{a2}}{2}\right)^2 - \left(\frac{d_{b2}}{2}\right)^2} - a_w \sin\alpha_w$	24

Contact ratio

$$\varepsilon_\alpha = \frac{g_\alpha}{p_b} = \frac{g_\alpha}{\pi \cdot m \cdot \cos\alpha} \quad (25)$$

Base tangent length (checking distance)

$$w_{1,2} = m \cdot \cos\alpha \left[\pi \cdot \left(z'_{1,2} - 0.5\right) + 2 \cdot x_{1,2} \cdot tg\ \alpha + z_{1,2} \cdot inv\ \alpha\right] \quad (26)$$

Number of teeth corresponding to the base tangent length

$$z'_{1,2} = \frac{\alpha}{180} \cdot z_{1,2} + 0.5 \quad (27)$$

Calculated gear profile parameters and their symbols are noted in the following Table 2. To help to understand terminologies used about tooth profile, following Figure 19 [12] shows the basic terms in a spur gear.

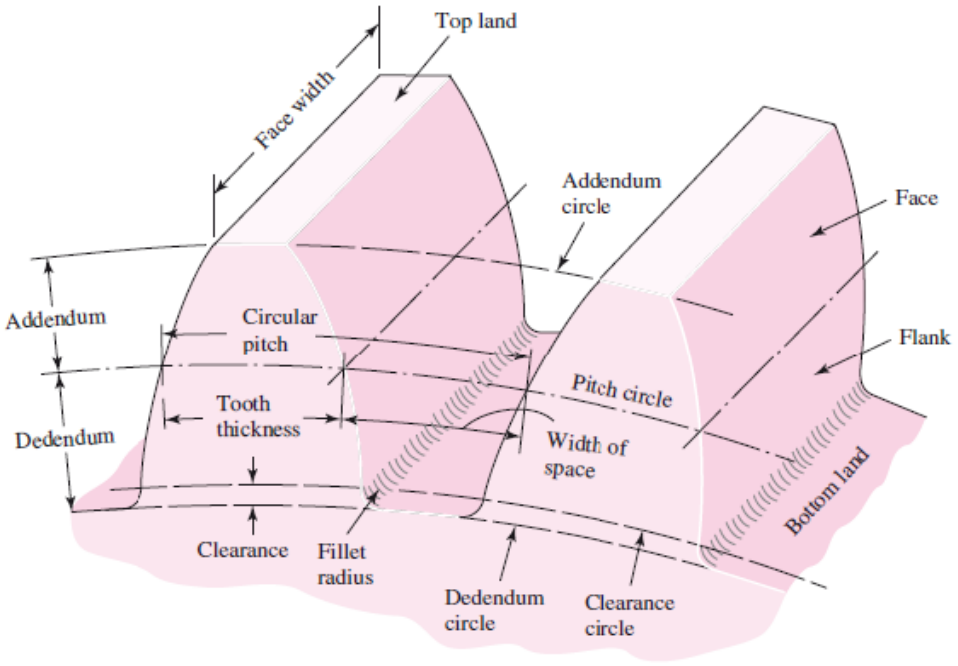

Figure 19. Terminologies of spur gear [12]

Name	Symbol	Value
Gear ratio	i	1.281
Pitch circle diameter	d_1	48.000mm
	d_2	61.500mm
Base circle diameter	d_{b1}	45.903mm
	d_{b2}	58.813mm
Center distance of the uncorrected pair of gears	a	54.750mm

Rolling pressure angle	α_w	17.000179°
Rolling circle diameter	d_{w1}	48.000mm
	d_{w2}	61.500mm
Center distance of the pair of gears	a_w	54.750mm
Basic rack tooth profile displacement	Δy	-0.000035mm
Height of addendum	h_{a1}	1.500052mm
	h_{a2}	1.500052mm
Height of addendum without correction	h_{at1}	1.500mm
	h_{at2}	1.500mm
Height of dedendum	h_{f1}	1.875mm
	h_{f2}	1.875mm
Total height	h_1	3.375mm
	h_2	3.375mm
Addendum circle diameter	d_{a1}	51.000mm
	d_{a2}	64.500mm
Dedendum circle diameter	d_{f1}	44.250mm
	d_{f2}	57.750mm
Circular pitch	p	4.712mm
Base circular pitch	p_b	4.506mm
Circle pitch on the rolling circle	p_w	4.506mm
Circular thickness of tooth	s_1	2.356mm
	s_2	2.356mm
Circular width of tooth space	e_1	2.356mm
	e_2	2.356mm
Length of the line of action	$\overline{AB}$	8.346mm
Contact ratio	ε_α	1.852
Base tangent length	w_1	14.034mm
	w_2	17.981mm
Number of teeth corresponding to the base tangent length	z'_1	3.522
	z'_2	4.372

Table 2. Spur gear tooth profile

With the calculated geometrical parameters, a pair of spur gears are minutely designed. The modeling has been done using CAD tool, Inventor. Then, they are imported into Abaqus as a form of step file. Their modeling space is on 3-D and the parts should have solid and deformable structures. The input and the paired output gear are present in Figure 20 and Figure 21.

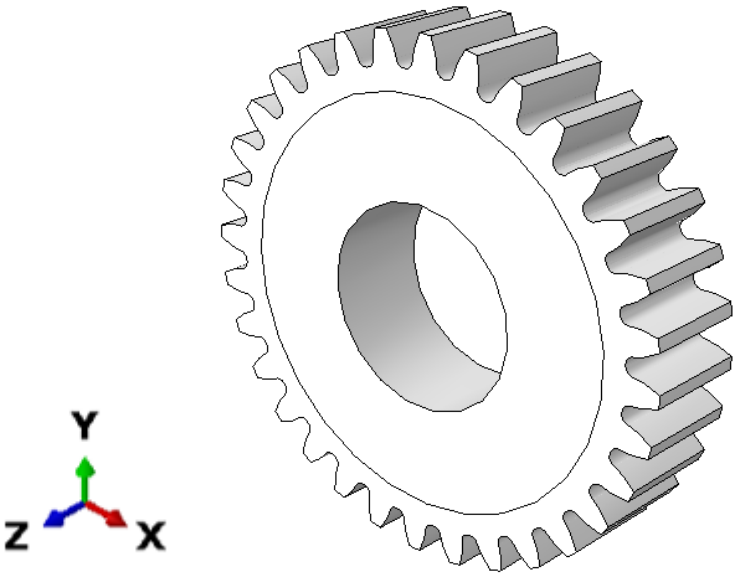

Figure 20. Part model of Gear 1

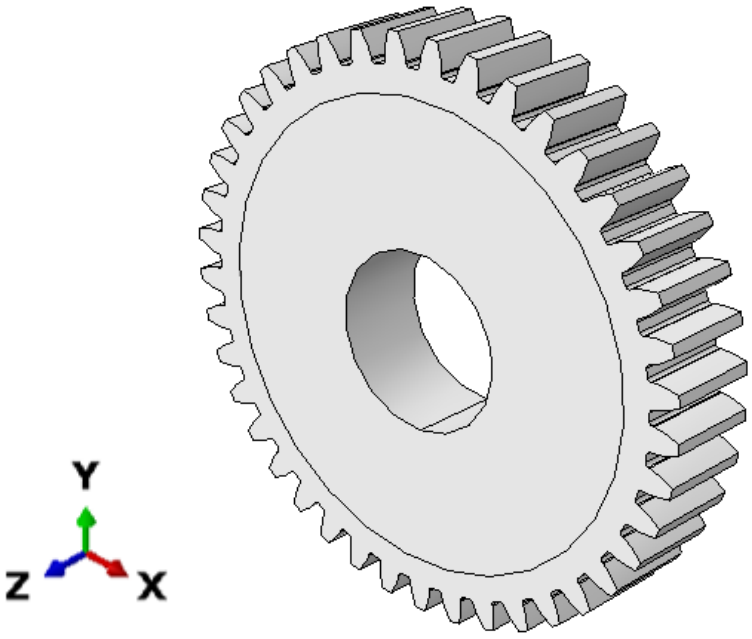

Figure 21. Part model of Gear 2

3.2.2. Material Property

As the next procedure, the material property of standard steel is applied to both gears. Abaqus program does not mark the unit, so the consistent units must be always in use. The values are re-calculating on basis of SI unit with mm. Thus the unit of the density is ton/mm^3 and that of Young's Modulus becomes $N/mm^2 = MPa$. On each gear, the following properties in Table 3 are assigned as a solid and homogenous type.

Material Property	
Density of driving gear (ρ_1)	7.85 ton/mm^3
Density of driven gear (ρ_2)	
Young's Modulus of driving gear (E_1)	210000 MPa
Young's Modulus of driven gear (E_2)	
Poisson's ratio of driving gear (ν_1)	0.3
Poisson's ratio of driven gear (ν_2)	

Table 3: Material Property

3.2.3. Assembly

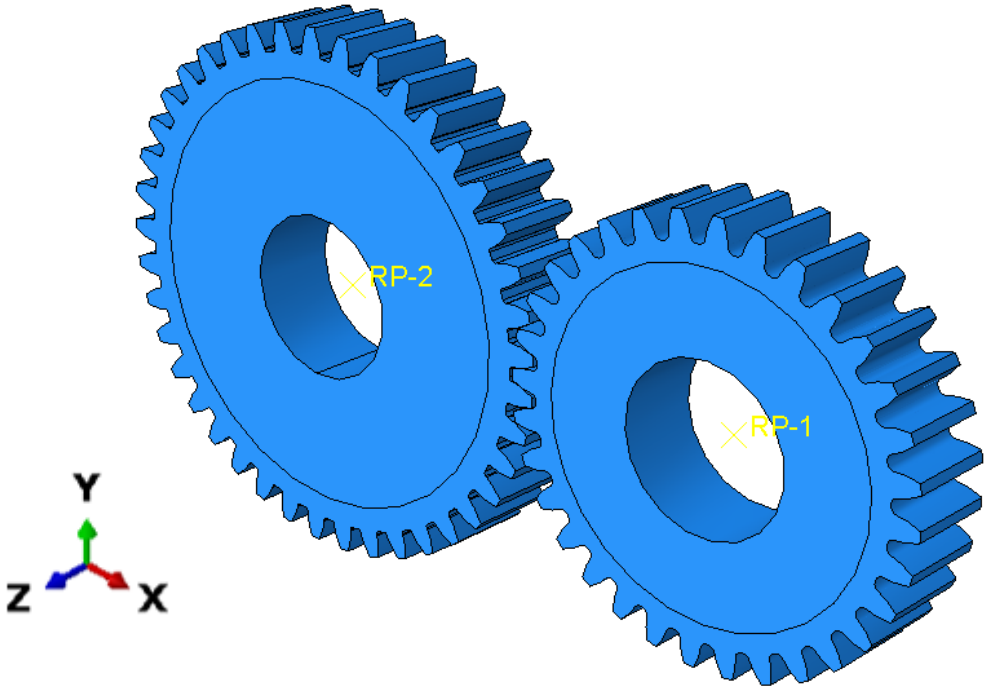

Figure 22. Assembly model of spur gears

In Figure 22 above, assembled model features can be found. The driving gear and the driven gear become instances of the assembly as a dependent part. The output gear is translated and rotated to the appropriate position following the values of calculated center distance between the centers of gears. To prevent the analysis from critical errors, initial overclosures must not appear between two parts. For the further procedure, two reference points are assigned to the center of each gear.

3.2.4. Step Definition

In this analysis, a dynamic explicit analysis is used which is computationally efficient for the analysis of models with short dynamic response times. This type of analysis allows a good result on a large number of small-time increments. The use of small increments that are dictated by the stability limit is advantageous because of the solution to proceed without iterations and without requiring tangent stiffness matrices to be formed.

When estimating the stable time increment size [13], an approximation to the stable limit is written as the smallest transit time of a dilatational wave across any of the elements in the mesh

Time increment size $$\Delta t \approx \frac{l_{min}}{c_{\mathrm{d}}}[s] \quad (28)$$

, where l_{min} is the smallest element dimension in the mesh and c_d is the dilatational wave speed. In the elastic model, this wave speed can be denoted as

Wave speed $$c_d = \sqrt{\frac{\lambda + 2\mu_s}{\rho}}\ [mm/s] \quad (29)$$

, where λ is Lame modulus and μ_s is the shear modulus. ρ denotes the density of the material which has tiny value due to the SI unit conversion. The stable time increment size becomes extremely small by the element size as well as the density of the material. Thus dynamic explicit mode is required to analyze this model.

At the same time, this FEM must be considered that the output has to have a higher sampling period to prevent the irregular change among each step. The speed sensor on the test stand has 10000 pulses per revolution and the maximum speed is approximately 5000rpm. It means the Abaqus sampling has to cover more than a certain number of samples calculated by the speed of the system and the resolution of the encoder.

Sample per second $$\frac{ppr \cdot rpm}{60\ second}\ [sample/s] \quad (30)$$

Thus, the output request should have approximately 1e-06 second interval to meet the condition. Fixed time incrementation is available in Abaqus explicit. This may be useful when a more accurate representation of the higher mode response of the problem is

desired. The characteristics of this dynamic explicit meet requirement to achieve TE because of the small-time intervals and stable increment.

The total analysis time in this dynamic explicit analysis is defined with the period of the event, which is enough time to obtain the stable behavior of meshing between the paired teeth. To obtain the result for the further calculation of transmission error, the velocity of the node on the central hole of each gear is set as output after the mesh is created on both features. Later, when the models get complex, the transmission shafts will pass through these holes, and on the tips of them will place the speed sensors. Also, to check the behavior of the output of the teeth, two more nodes are placed on the tip. In Figure 23 below, these 4 assigned nodes are marked with red dots. Also, the stress output and the deformation output are requested to see what is happening during the calculation and to see if there is a fluent contact. The Nlgeom (Non-linear geometry) should be on to predict characteristics of the deformable gear model accurately.

However, it can cause extreme time consumption and overlarge output memory by the number of mesh and the number of required output data. It is not desirable to take such an effort to proceed to further study. As a solution to this, the partitions are created to assign different mesh size and to minimize the mesh number by increasing the mesh size within a reasonable range. Another solution can be to pick the minimum outputs required. Therefore, the output variables which are out of concern, such as acoustics and porous media are canceled to be shown on the result. When the finite element model is certainly created, the domain of analysis can be also decreased from the entire model to the assigned set such as the nodes. By these means, the total memory and time consumption which are drawn by the total step could be diminished, since the calculation is conducted only toward the target.

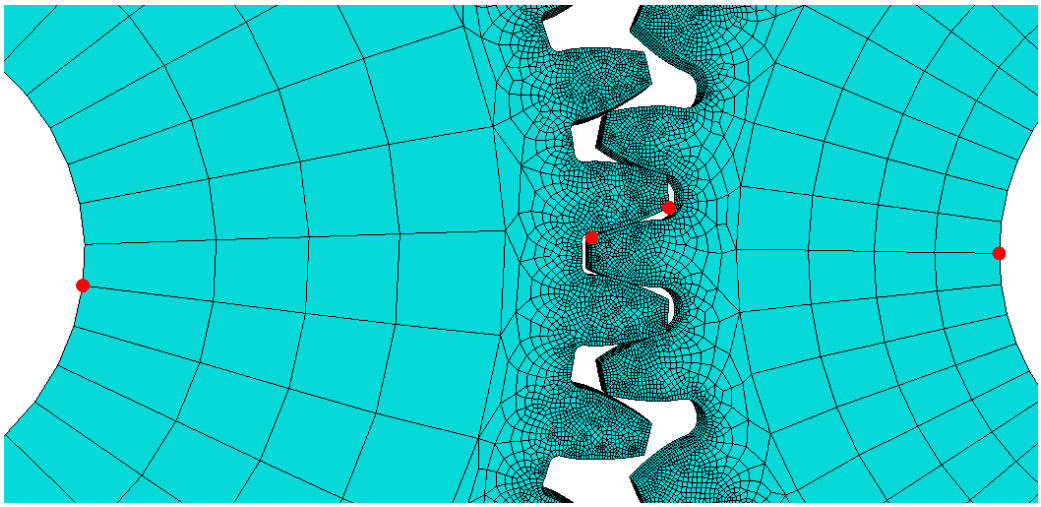

Figure 23. Picked nodes for sampling

3.2.5. Interaction

As constraints, kinematic couplings are added and all degrees of freedom were toggled on to constrain. The control points are assigned on each reference points and the

constraint regions are the inner surfaces of bores where the shafts will be assembled.

By creating interaction with the explicit general contact, Abaqus specifies the contacting surfaces automatically and conducts the calculation based on the contact properties. This default surface contains all analytical surfaces and all exterior elements faces in the entire model. It should ensure that all contacted surfaces on teeth are chosen during a given period so that while the gears rotate, contacts on some surfaces are not missing.

When surfaces are in contact, they transmit shear and normal forces across their interface as known as the friction. To define ideal friction can be very complex since it has several options and can cause different errors without using a proper mode and an appropriate value. Abaqus provides frictionless by default, penalty, exponential decay, and Lagrange friction models. Coulomb friction is a common friction model which is used to describe the interaction of contacting surfaces. This model can be largely classified into a dry model, a viscous model, and an elastic model. Figure 24 [14] is an illustration showing the relationship between the frictional force and the relative velocity of relative displacement of the contact surface in the dry model, and the elastic model. In the case of the dry model, when the relative speed is zero the friction force corresponds to the magnitude of the external force acting on the contacting object and once the relative speed occurs the friction force corresponds to the multiplication of the friction coefficient and the normal force. This can be expressed by the following equation.

$$\textbf{\textit{Dry model frictional force}} \qquad F_t = \mu N\ [N] \qquad 31$$

F_t is a frictional force where μ is a friction coefficient and N is a normal force on the surface. The contacting surfaces don't slip until the shear stress equals to its critical value. This behavior shows an abrupt step motion as shown in Figure 24 on the left-hand side. No relative slip motion exists on the surfaces when they are contacting. This implies numerical instability due to discontinuous changes in the friction force. This discontinuity can cause convergence problems during the simulation. The specific friction model should be introduced to observe the response of the model

Therefore, the elastic Coulomb friction model is assigned, which allows the elastic slip of deformable bodies. The behavior of this model is shown in Figure 24 on the right-hand side. In this case, even if the contacting object is in an adhesive state it is assumed that a small amount of relative displacement occurs. The friction force is proportional to the amount of sliding and it is defined as in the following equation.

$$\textbf{\textit{Elastic model frictional force}} \qquad F_t = \frac{\mu N}{l_0} S\ [N] \qquad 32$$

S is a sliding amount and l_0 is an amount of critical elastic sliding, which is the value when the frictional force reaches the threshold. As it is obvious by the figure, the stiffness of the sliding generated between the two surfaces is closely related to the critical elastic sliding amount. Considering the material and the lubricated environment under the high rotational speed, the value of the friction coefficient is defined 0.1 in this analysis.

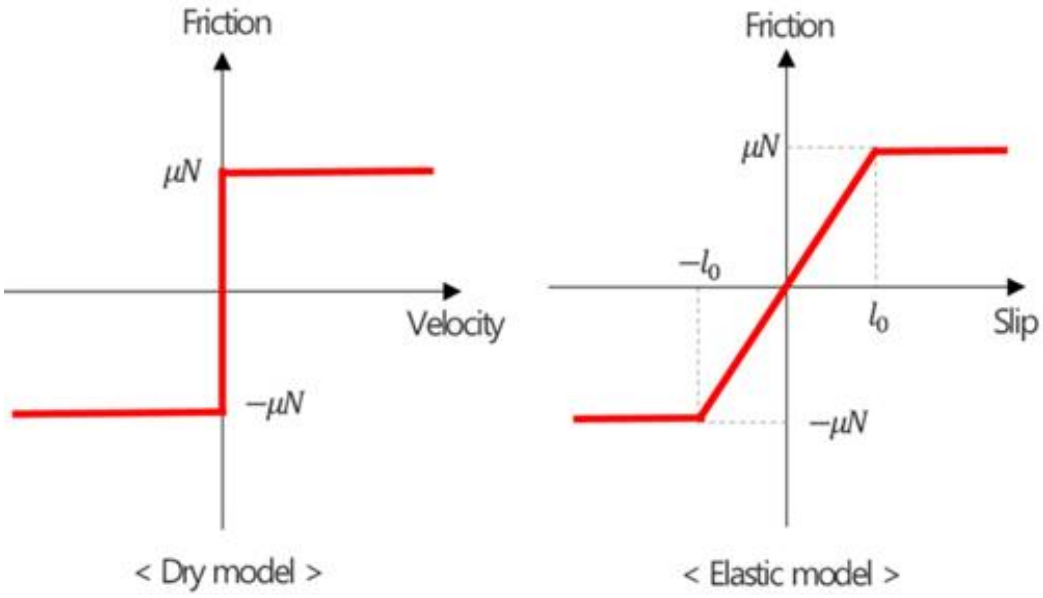

Figure 24. Frictional behavior [14]

The most common contact relationship is shown in Figure 25 [15]. Hard contact implies that there is no penetration between the surfaces when no contact pressure exists either. It means when the gears are rotating, the contact pressure might become zero as the faces are separated and the clearance between two contact surfaces becomes larger than zero. At the same time, the contact nodes and the restraints separate as well. At the very moment the surfaces meet, any contact pressure can be transmitted between them. This behavior is to be expected as a logical course of events. Thus, this model follows hard contact as its normal behavior.

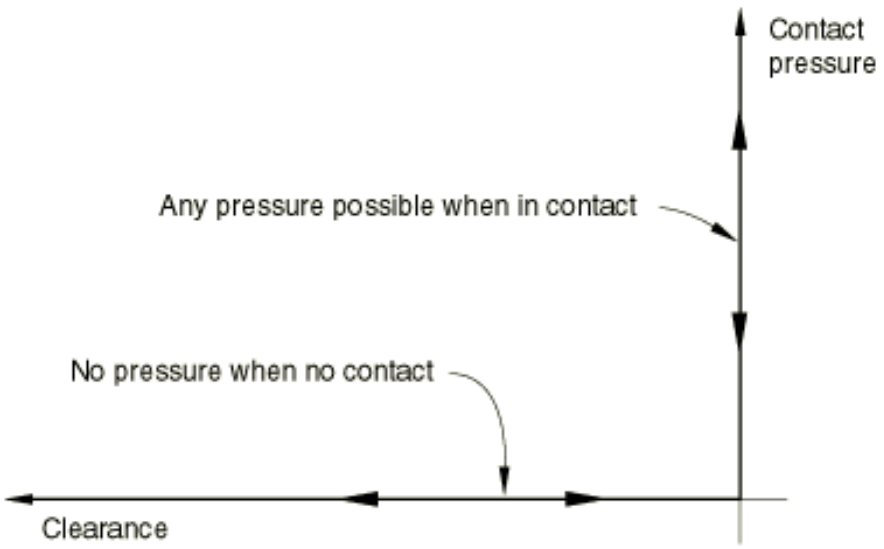

Figure 25. Hard contact relationship [15]

3.2.6. Load and Boundary Condition

In this module, loads and boundary conditions are defined. The driving gear rotates around 1250 rpm which is 130.9rad/sec in accordance with the unit in Abaqus. This angular velocity should have a time delay to avoid a severe error, which is further explained in the "Trial and Error" section. The amplitude of velocity gradually increases until it reaches its maximum point with a time lag. The driven gear doesn't have prescribed angular velocity, but its rotation has to be guaranteed on the rotating axis of the gear set. Simultaneously the driven gear has 120 Nm (120000Nmm) of torque against the direction of the rotation of the input gear. All of the kinematic properties should be assigned on each corresponding reference point which locates in the centers of gears.

3.2.7. Mesh

In finite element analysis, the mesh of the parts is the key to achieve the desired result. The hexahedral shape of the C3D8R mesh element type is generated since it has a good ability to capture the complex geometry of the model. As it is mentioned in the "Step" chapter, the partitions are created on these test parts to decrease computation time.

All of the teeth must contain fine mesh to run Abaqus calculation until the behavior becomes stabilized after initial excitation by speed and torque assignment. This fine mesh detail is already shown in Figure 23 in the "Step" section with the specified node-set. The mesh structure on total assembly is shown below. The element size along the profile is approximately 0.1mm. And it is clear that other elements are in concentric shape from the center and their size is visibly bigger in the following Figure 26. This helps the calculation to spend much less time in the boundary that the result still can end reliably. The total node number of the input gear (right) is 57292 and that of the output gear (left) is 81720.

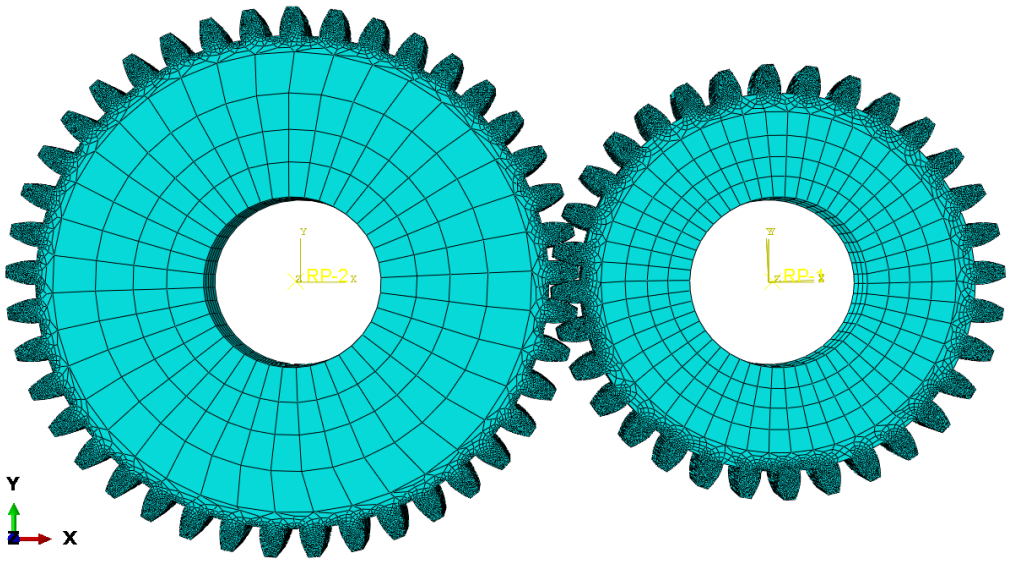

Figure 26. Generated mesh on spur gears

3.3. Result

3.3.1. Abaqus

Once the analysis is finished until the model maintains its behavior, the required outputs by the user can be plotted or listed on the table. One of the main outputs, the translational velocity is graphically shown at a certain moment in Figure 27. It shows velocity distribution on gear geometries and its unit is mm/s by the Abaqus default unit. Owing to the stress along mesh line between teeth is changing and the effect reaches the center of gears, the amount of velocity on each part of the gears differs from time to time. This is one of the critical factors which causes the transmission error due to the deformation. It results in a form of displacement difference among the teeth and the inconstant velocity as expected.

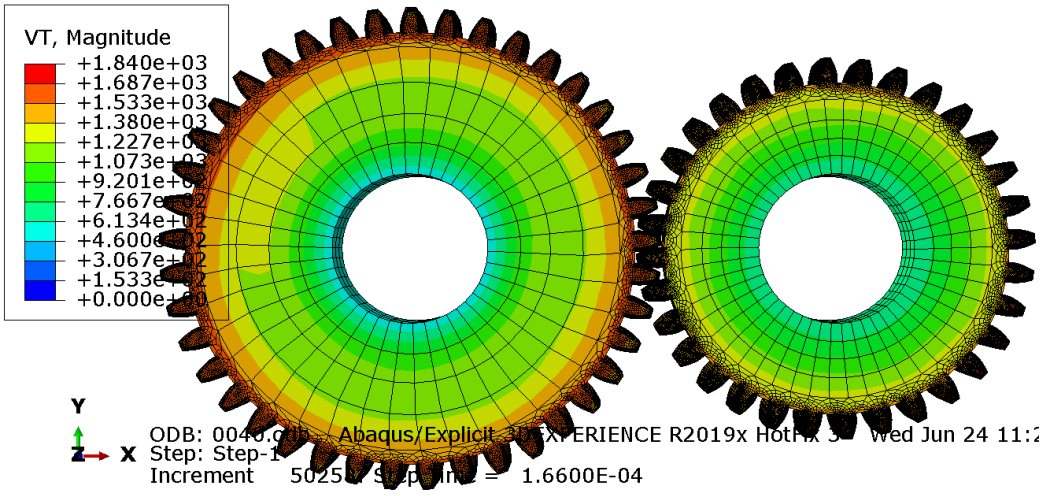

Figure 27. Velocity distribution on spur gear model

Figure 28 below is the raw material directly exported from the Abaqus since it is not calculated any further yet. Velocities of two nodes on each gear bores have been plotted, which are pointed out in the “Step” module. The line that has an approximately constant value on the graph indicates the velocity on the input gear hole because the initial velocity is assigned on the input gear hole. The velocity on the output gear has a large fluctuation by the initial conditions. Until it settles, the transmission error is also led to having unstable fluctuation. Afterward, it tends to behave more stably. At this moment, the plot can be exported as a form of Excel sheet by using Abaqus plug-in. In the Excel file, the component of each node on bores and the time should be properly named to ease the next step with DIAdem. The further TE calculation will be dealt with in the next chapter.

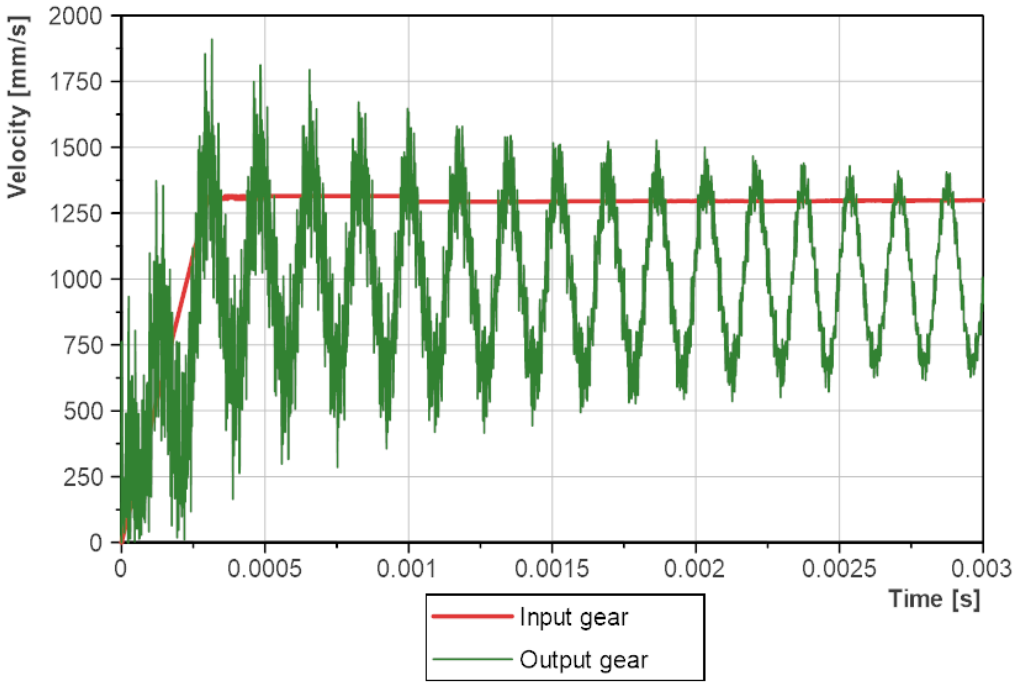

Figure 28. Velocity on sampled nodes at 1250rpm

3.4. Conclusion

As the guidance and as the first step of the whole thesis, this chapter has been conducted with a simple spur gear model. It allows us to acquire knowledge and to set the direction regarding this study. This model has introduced the instrumental program and the main result from the finite element method has been shown to obtain transmission error for the next chapter. From the basic gear profile calculation to data acquisition, each step by step process is established. It has been checked whether the analysis using Abaqus has conducted successfully. The rotation of the paired gears goes well and gear meshing lies all right on the pressure line. The speed and stress of the parts correlate the moment when the teeth mesh one another so the fluctuating velocity graph by nodes has been acquired.

To minimize any elementary mistake and to be familiarized with the finite element method, rough analysis is conducted as a test version. Based on this methodology, the next chapter will have proceeded with the usage of a helical gear set in a similar manner. In addition, data processing by NI DIAdem will be introduced and the transmission error will be calculated which has not been undertaken in this chapter.

4. Transmission Error of Simplified Helical Gear Model

4.1. Introduction

In this chapter, a new model is introduced with a helical gear pair. The creation of the new parts and the additional calculation are included. The gear design is more elaborated based on the drawings of real parts that are used on the test rig in the laboratory. The following result is expected to be more similar to the output from the experiment because of the part adaption. Like the previous chapter, the finite element method is conducted by Abaqus and DIAdem is used for data processing.

4.2. Finite Element Analysis of Helical Gear

4.2.1. Model Creation

The parameters of actual gear wheels, which are utilized on the test bench are known. Below, the main gear parameters in the translated tables from the original German version are placed and re-organized to Table 4 and Table 5 describing both gears. Original tables and additional data can be found in annexes.

Before the design stage of the machine parts, it is necessary to understand the new information about the profile shift factor. The factor has a certain relationship with its manufacturing process which is well known by milling, slotting, shaping, or hobbing. The finishing process can be done by shaving, grinding, burnishing, or lapping. The most frequently used tool to generate a gear profile is a rack cutter. It has its basic profile and a module. When the rack cutter reciprocates with feed, there comes the point that its pitch straight line reaches the rolling straight line and the rolling circle becomes the same as the pitch circle of the gear. This is the way an uncorrected gear is generated.

On the other hand, gears may have corrections. The gear tooth correction makes the displacement of the rack pitch straight line from the uncorrected position. When the rack penetrates more into the gear blank, it has a negative correction and vice versa. This tooth correction is expressed with the multiplication of the module and the profile shift factor. The amount of profile shift generates a different profile of gear by an extra feed toward the gear or a spare distance from the original position. Profile shifting is applied to create gears with different tooth thickness, which makes differences from standard gears. Due to this variation, the gear strength and the center distance between two gears are changed as well. When the negative profile shift factor is applied, the tooth thickness decreases and tip diameter decreases, causing a reduction of the center distance. To adapt this new parameter to the system, a few additional calculations are needed. These values of extra parameters are calculated in Table 6 and the equations to derive them are described above the table.

Input gear parameter	
Module (m_1)	1.5mm
Normal pressure angle (α_1)	17°
Helix angle (β)	32°
Number of teeth of input gear (z_1)	32 (right-handed)
Profile shift factor (x_1)	0
Addendum circle diameter (d_{a1})	61.30 mm
Dedendum circle diameter (d_{f1})	52.60 mm
Base circle diameter (d_{b1})	53.2461 mm
Pitch circle diameter (d_1)	56.6006 mm
Flank width	18 mm
Bore diameter	35.30 mm

Table 4. Input helical gear parameter

Output gear parameter	
Module (m_2)	1.5mm
Normal pressure angle (α_2)	17°
Helix angle (β)	32°
Number of teeth of input gear(z_1)	41 (left-handed)
Profile shift factor (x_2)	-0.04
Addendum circle diameter (d_{a2})	76.450 mm
Dedendum circle diameter (d_{f2})	67.75 mm
Base circle diameter (d_{b2})	68.2215 mm
Pitch circle diameter (d_2)	72.5195 mm
Flank width	18.5 mm
Bore diameter	34.25 mm

Table 5. Output helical gear parameter

Due to profile shifting, the central distance is also shifted, since the addendum and the tooth depth differs. When the gear has a positive correction, it enlarges the center distance and reduces the center distance in case of the negative correction. This profile requirement must be well adapted to the gear teeth design. Hence, the creation of helical gears is done with a gear generating tool in Abaqus for a better geometrical detail accepting extra parameters. This gear generator is a plug-in tool and it is necessary to be downloaded through Dassault Systèmes. The assembly model of helical gears can be found in Figure 29.

In the property module in Abaqus, the same material property which is used in the spur gear model such as Young's modulus, Poisson's ratio, and density is added on the driving and driven gear.

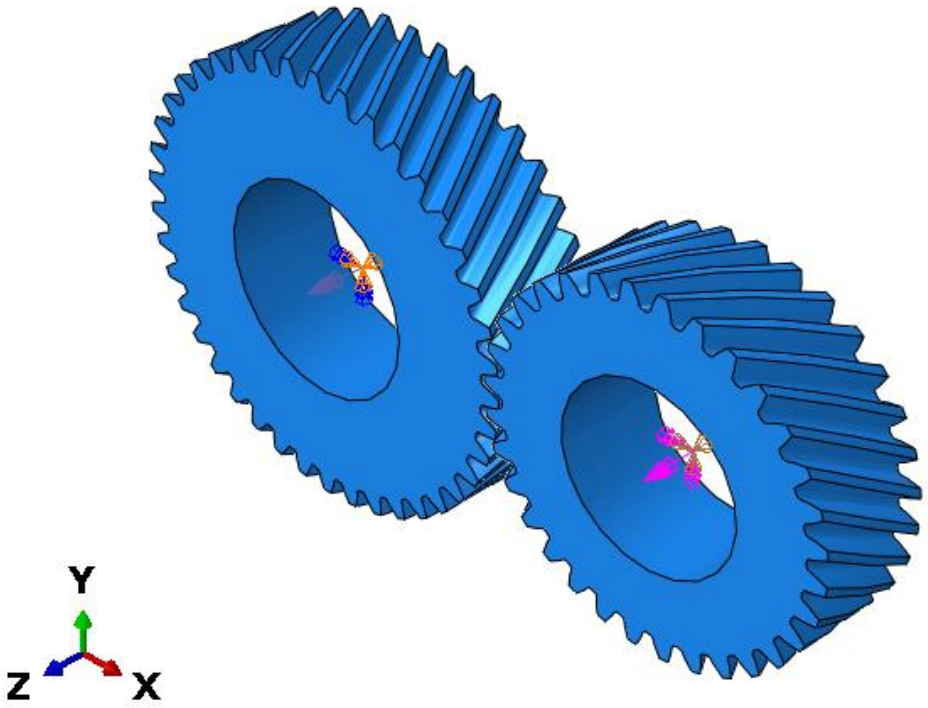

Figure 29. Assembly model of helical gears

Transverse pressure angle $$\alpha_t = tan^{-1}\left(\frac{\tan\alpha}{\cos\beta}\right) \quad (33)$$

Involute function of α_{wt} $$inv\ \alpha_{wt} = 2\tan\alpha\left(\frac{x_1 + x_2}{z_1 + z_2}\right) + inv\ \alpha_t \quad (34)$$

Center distance modification $$y = \frac{z_1 + z_2}{2\cos\beta}\left(\frac{\cos\alpha_t}{\cos\alpha_{wt}} - 1\right) \quad (35)$$

Corrected center distance $$a_c = \left(\frac{z_1 + z_2}{2\ cos\ \beta} + y\right)m \quad (36)$$

Modified parameters	
Transverse pressure angle (α_t)	19.825°
Involute function of α_t	0.015
Involute function of α_{wt}	0.014
Transverse working pressure angle (α_{wt})	19.680°
Center distance modification (y)	-0.039
Center distance (a_c)	64.502mm

Table 6. Modified parameters

4.2.2. Interaction and Load

Interactions are settled following the methodology in the spur gear model as well. The friction contact and hard contact are applied in certain conditions. Coupling constraints are assigned to couple the motion of a collection of nodes on the bores and the motion of the reference points in the middle of each gear. For the kinematics, the load on output gear is 120000Nmm and the 130.9 rad/s (1250rpm) angular speed on input gear is applied the same as the test rig example. Additionally, one more analysis is conducted with a speed of 209.44rad/s (2000rpm) to see the different effect on TE. Because of the reason which will be introduced in a few chapters, the delay on input gear speed is necessary. When the faster the initial velocity is, the longer delay should be assigned to compensate elastic collisions by a rapid change.

4.2.3. Mesh and Step

As the analysis is dynamic/explicit, element type has to be also for explicit analysis. The fine hexahedral mesh is generated intensively on the tooth profile of both gears as shown in Figure 30. Elements are swept along the helical angle. This time, the quality of the mesh is more important than the calculation time, since this FEM is full-scaled. It has the propagating shape from the smallest 0.1 sizes of elements to bigger elements around the bore. The total number of elements in input gear is 89932 and that in output gear is 98292. Abaqus/Explicit offers distortion control. It is used to prevent solid elements from inverting or distorting excessively. Also for better results, the hourglass control method is combined with it.

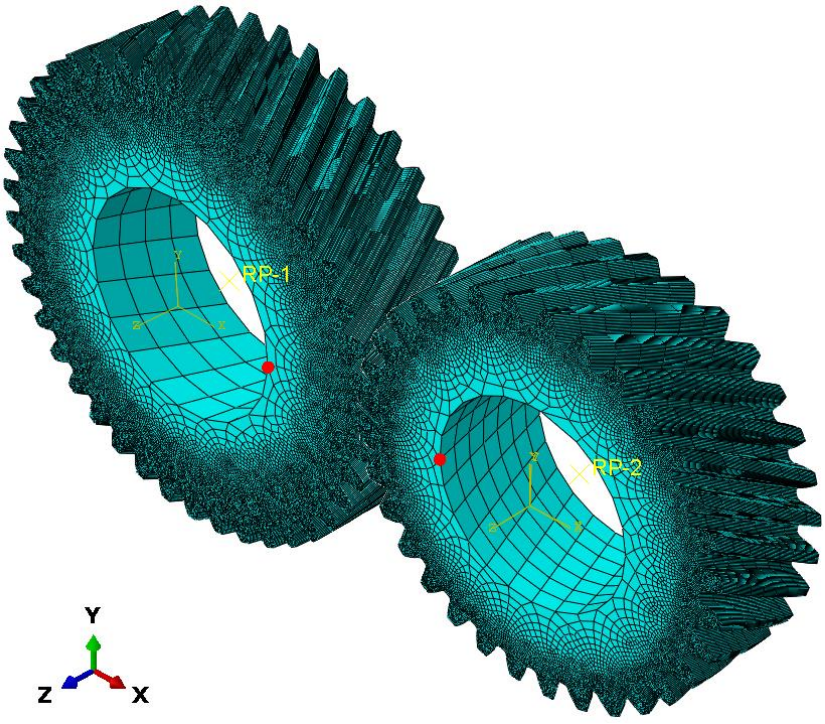

Figure 30. Generated mesh on helical gears

At step module, information of nodes on the bores are collected in the step period similarly to the spur gear model. Two nodes that are selected can be seen as red dots on bores in the generated mesh on helical gears. Other parameters that are not related to transmission error are excluded from the output requirement. According to the angular velocity, the step time is also appropriately adjusted.

4.2.4. Trial and Error

While running several computational experiments some problems have popped up as well. As the helical gear model runs for a longer step period and higher velocity, other unexpected issues have found on analysis. The compensation of the defects is already reflected in the previous modeling chapters but it is worth noting the reason and the solution to eliminate the question marks.

The first issue is about the opposite stress distribution on the tooth profile. It could be found out as the stress output is checked to be shown. In the dynamic analysis, when the simulation has started the system is in an unsteady state due to the inertial effects and also the elastic collisions as a result of the contact interaction properties chosen before. When the velocity is applied at a sudden moment, in the beginning, it causes an abrupt and massive deformation on the reacting part, in this case, the teeth of the output gear. This effect has appeared as a form of different stress direction on the teeth. In Figure 31, the result of rebound motion can be found in the opposite direction of normally applied stress. The stress is supposed to act like the picture on the left-hand side because the input gear on the right-hand side is rotating in a counterclockwise. Theoretically, the pressure line should lie on the upper right side to the lower left side as, in normal operation. However, as it is shown on the picture on the right-hand side, the force is applied in a different direction. This implies that the sudden deformation on teeth may cause the rebound to move the teeth back to their position.

For this reason, an abrupt initial condition should be avoided as much as possible, since it may bring instabilities to the whole simulation. To prevent the radical excitation at the beginning of the analysis, a ramp-up delay is introduced to the angular velocity. This can gradually increase the velocity up to the assigned amount from the zero value. Long enough delay could prevent the output gear from the rebound incident caused by smoothening the initial velocity. However, an extremely long delay is not desirable because an additional increment on total time is needed to see TE in stable status. Then the analysis would take much unnecessary time and memory. By a few experiments, a reasonable delay time is found as described in the following Table 7.

Time delay on different input velocity		
rpm	rad/s	delay
1250	130.9	0.00035s
2000	209.44	0.0005s

Table 7. Time delay on different input velocity

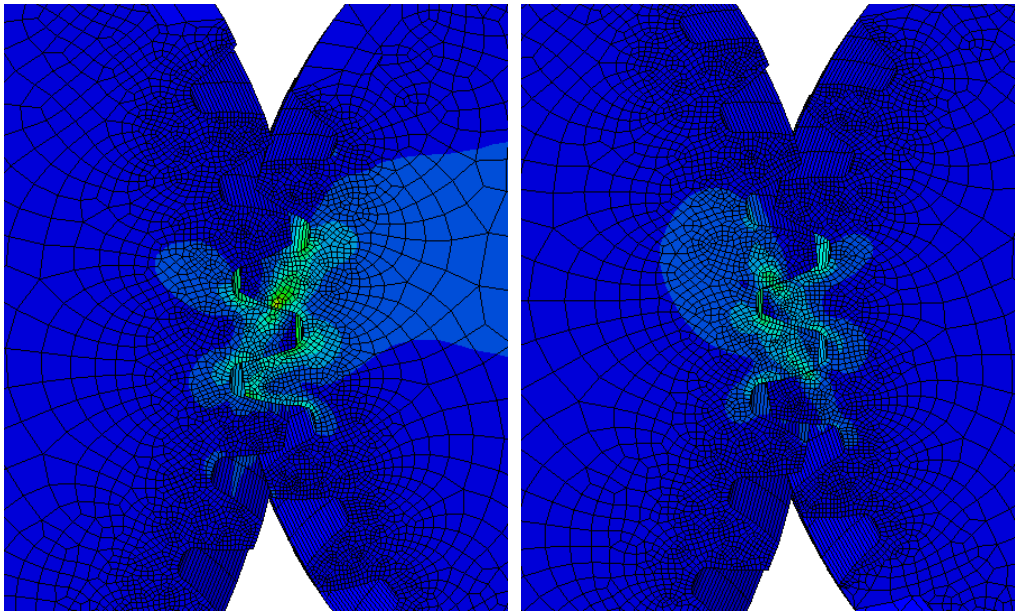

Figure 31. Normal stress distribution(left) vs Stress distribution during rebound (right)

The other error that also occurred in the model was the hourglass mode. It is accompanied by the excessive deformation on a single mesh component, as it is shown in Figure 32 below. The viewpoint is adjusted and showing just one gear to demonstrate the situation better. This hourglass mode leads to immature abortion of total analysis. The shape of teeth look wavy and deflected in an irrelevant way to the motion of parts. Also, the stress distribution is not clear on the pressure line of the gear and teeth are not in contact with paired ones. Both of the gears have shown this wavelike deformation which is developed on teeth profile.

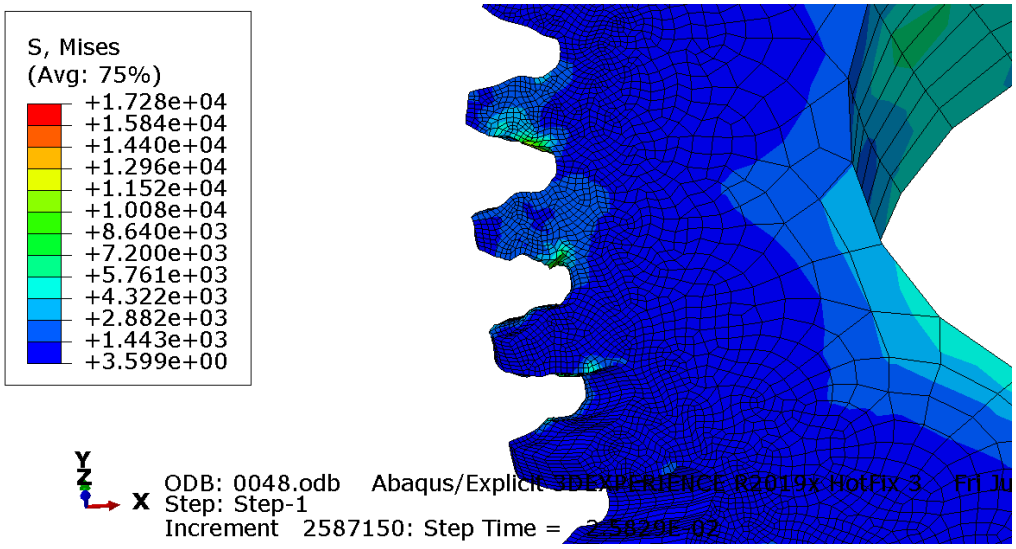

Figure 32. Severe distortion on elements

In order to understand this phenomenon, element type in Abaqus has to be understood. The element type can be divided into a full integration element and a reduced integration element. At sampling points which are called integration points in element,

the stiffness and mass of an element are numerically calculated and the numerical algorithm works to integrate the influences of these variables based on the way that an element behaves. As it is arranged below in Figure 33 [16], different order interpolation can be applied as well. The number of nodes in an element determines how the nodal degrees of freedom will be interpolated over the domain of the element.

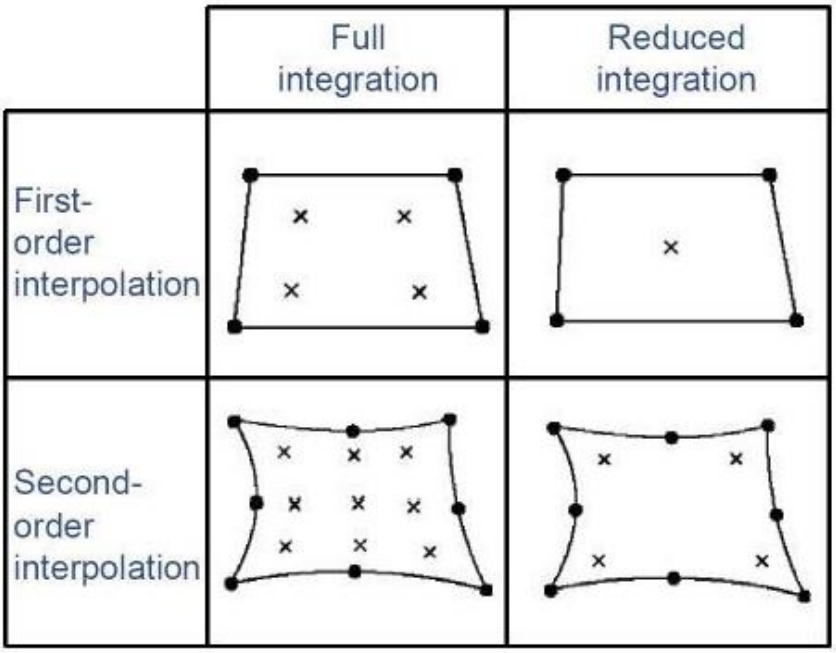

Figure 33. Abaqus element type [16]

In this analysis, C3D8R elements are assigned and it indicates by the name that reduced integration elements are used. There are several advantages of the usage of reduced integration elements. One is that the strains and stresses are calculated at the locations that provide optimal accuracy even compared to other types of elements. Also, it decreases CPU time and storage requirements, since it doesn't require many calculations in comparison with full integration elements. However, reduced integration may cause a severe disadvantage as well. During this integration process, the deformation mode that causes no straining at the integration points is allowed. This is so-called hourglassing, where the zero-energy mode propagates through the mesh, leading to inaccurate solutions. The error which occurred on the gear models also attributes to the hourglass effect.

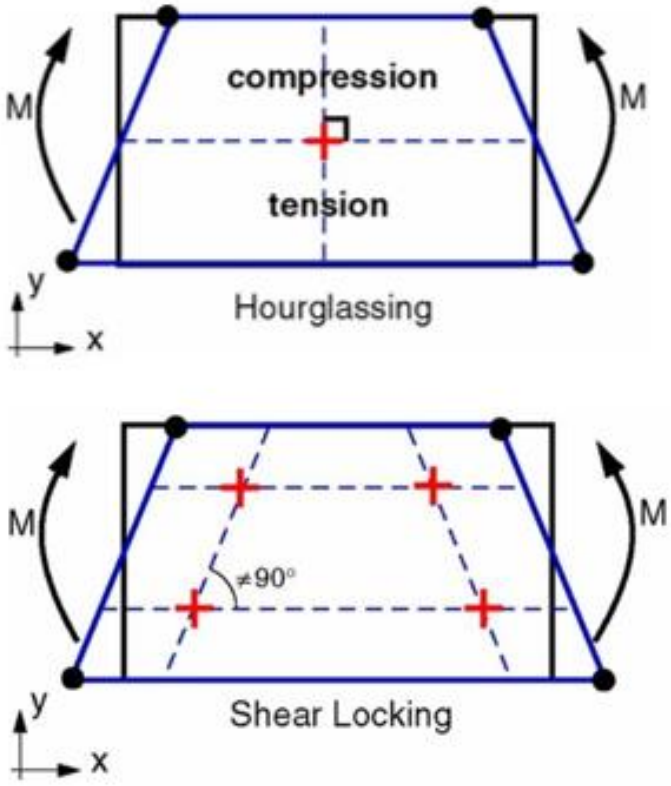

Figure 34. Hourglassing (top) and Shear locking (bottom) [17]

To elaborate, Figure 34 [17] shows the idea of the hourglass effect on the top side. It is a mesh instability that affects first-order reduced integration continuum elements and reduced integration elements. Due to that, first-order reduced integration elements cause no strain energy at the integration point as it is shown on. Crossing the center point, there is no change in length, as shown with dashed lines even though the tension and compression occur on the element by the bending moment. Hence, a single element through the thickness cannot detect the strain in bending. This may lead to severe mesh distortion with no stresses resisting the deformation.

To overcome this problem, some possibilities exist by modification of the finite element model or mesh element type. Mesh can be re-created from coarsely to finely. This can be a simple solution but it drastically increases the cost on time and this is not so ideal when the number of elements is limited. In another way, viscosity can be additionally applied to compensate for the artificial strain energy. However, there is a problem to find a reasonable value of viscosity. When the value is too little, it would not be able to diminish the hourglass effect. On the other hand, too high viscosity may affect the analysis result and it is not desirable. The third method is to change the element type from first-order reduced element to full integration element, but another problem called shear locking can arise by this method. On the bottom side of Figure 34, the elements detect shear strains at the integration points because the angle between the deformed lines is not equal to 90°, since the edges of the element must remain straight. It results in overly stiff behavior by the energy going into shearing the element rather than bending. Therefore these elements are not suitable in regions where the bending

dominates like tooth profile. At last, the hourglass control can be attempted to minimize these problems without introducing excessive constraints on the element's physical response. Abaqus has built-in hourglass controls that limit the problems caused by hourglassing. It verifies that the artificial energy which is generated because of the hourglass effect is less than 1 percent of the internal energy.

4.3.Result

4.3.1 Abaqus

Before the transmission error is calculated, it has to be ensured that both parts are rotating without any penetration or rebound motion. Then the time versus magnitude of translational velocity data is obtained by Abaqus. With the Abaqus plug-in tool, these values are converted to Excel data.

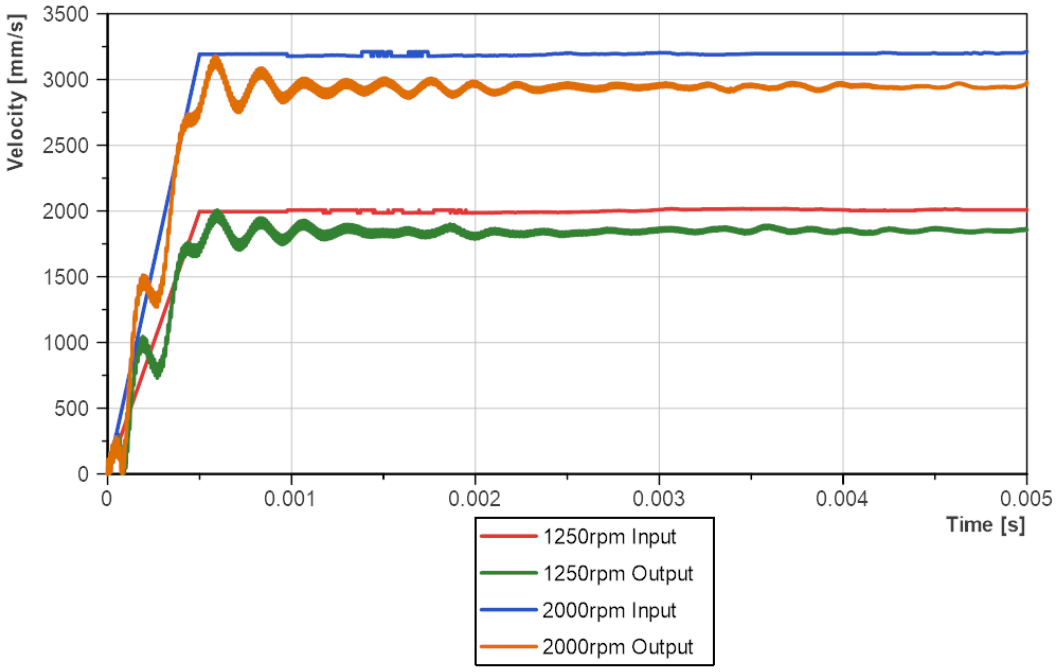

Figure 35. Velocity of nodes at 1250rpm and 2000rpm

Figure 35 above shows how the velocity on nodes on the bores' behavior. Ramp-up time delay is evident on both of the speeds. Node on the input gear remains approximately the same amount of velocity which is proportional to the initial angular velocity. Indicated speed is about 1996.225mm/s at 1250rpm and 3193.96mm/s at 2000rpm. There are small bumps on the initial phase and it soon settles down. The velocities of elements on output gears oscillate due to the reaction on initial excitation. As time goes by and the input angular velocity stays nearly constant, the fluctuation on output gear diminishes by time.

4.3.2 NI DIAdem

As the rough calculation has been mentioned in the first introductory chapter, the transmission error occurs by the difference between arc lengths of tangent circles. The length of each arc can be calculated by the multiplication of the rotated angle in unit time and the length of the pitch radius. In this study, the velocity on each gears' bore is derived as an output. So the velocity on the bore nodes and the step time should be concerned instead of the angle in Equation 3. The angle can be derived from the integration of translational velocity by time. The ratio of the pitch radius and the bore radius has to be multiplied since the velocity output is from bore radius, not from pitch radius. This can be expressed as the following equation.

$$L = r\,\theta = \frac{r}{r_{bo}} \int v_{bo}\ dt \tag{37}$$

$$(r = pitch\ radius, \quad r_{bo} = bore\ radius\ )$$

$$(\theta = rotation\ angle, \quad v_{bo} = velocity\ on\ bore, \quad t = time)$$

Variables of the pitch radius, bore radius, and the angular velocity by time are now known by the created parts and the obtained output, each arc lengths for a given time can be calculated. If the displacement difference between those lengths exists, it indicates transmission error on gears.

$$TE \qquad L_{1,real} - L_{2,real} = \frac{r_1}{r_{bo1}} \int v_{bo1}\ dt - \frac{r_2}{r_{bo2}} \int v_{bo2}\ dt \tag{38}$$

Numbers 1 and 2 represent the input gear and the output gear respectively. Once the velocity data by time is imported to DIAdem, a well-structured script can help to calculate the Equation 38. The script is written in Figure 36 and obtained TE can be plotted like Figure 37. Transmission error in initial condition has been excluded and the only stable result is shown.

```
'Helical gear TE'
Set ChnResult = ChnIntegrate("[19]/Time","[19]/Input_hole","[19]/alphal","TrapezoidalRule",0,0,0)
Set ChnResult = ChnIntegrate("[19]/Time","[19]/Output_hole","[19]/alpha2","TrapezoidalRule",0,0,0)
Set ChnResult = ChnLinScale("[19]/alphal","[19]/L1",(28.3003/15.25),0)
Set ChnResult = ChnLinScale("[19]/alpha2","[19]/L2",(36.25975/18),0)
Set ChnResult = ChnSub("[19]/L1","[19]/L2","[19]/TE")
```

Figure 36. TE calculation script for helical gear model

Finally, the transmission error is visualized as a time-domain graph. In Figure 37, transmission error in two different speeds are plotted. The first millisecond is excluded due to transient behavior by analysis initialization.

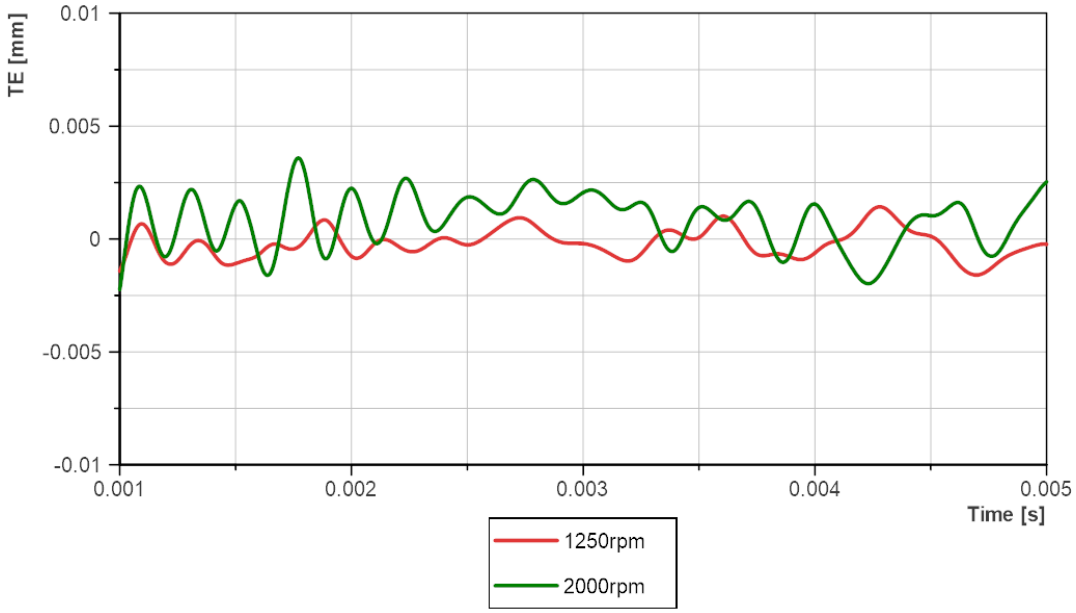

Figure 37. TE of helical gear model at 1250rpm and 2000rpm

When it comes to the tendency of TE on both speed, it seems that the oscillation at 2000rpm is more noticeable. With the same assigned torque on output gear which is against the angular movement of this model, higher input velocity on input gear may give rise to a huger deformation.

To verify that the transmission error corresponds to the gear meshing of the parts, a frequency-domain graph needs to be introduced. The next following Figure 38 contains frequency domain graphs at two mentioned angular speeds. The amplitude becomes trivial at a higher frequency, so the range is adjusted. Gear mesh frequencies are marked on each graph. In a low-frequency zone which is near to 0 Hz, high peaks occur on both speeds due to the initial fluctuation. The amplitude peaks are not closely distributed and seem to be scattered. It is because the frequency sideband is wide about 5e05 Hz because of the high sampling frequency and the total time is not long enough to create dense frequency increment. Still the peaks can be found in the vicinity of GMFs.

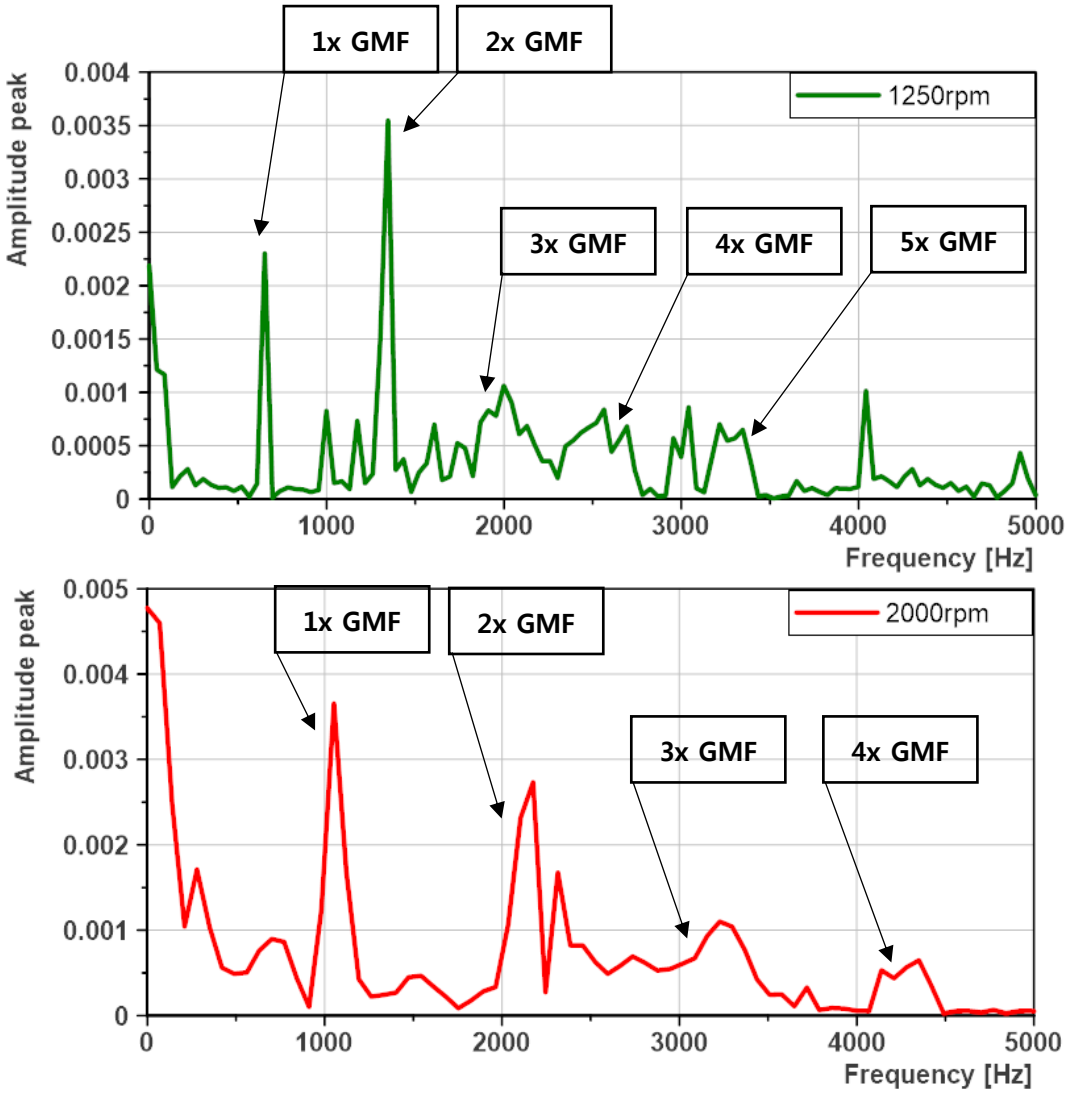

Figure 38. Frequency domain of helical gear model at 1250rpm (top) and 2000rpm (bottom)

4.4. Conclusion

In this present chapter, a similar methodology which is learned by spur gear is conducted targeting helical gear pair. New elaborated gear parts and the additional calculations for the changed parameters are introduced. Most importantly, the trial and error section has shown possible errors in dynamic analysis that can be critical to the result. It has also introduced the reasons they occur and the solutions which may resolve the problems. After data acquisition, transmission error at two different speeds has been compared and the result has been contemplated. As a suggestion of more informative research, the TE can be calculated with results at various input speeds and comparison depending on it can be undertaken.

5. Transmission Error of Complex Helical Gear Model

5.1. Introduction

As the transmission error is a mutual interaction among the parts, the analysis of the complex model is essential. Therefore, the complex helical gear model is created to make the finite element method relative to reality in a better way. This model contains more details as the additional components are adapted. Additional analysis with low speed has been conducted to see the static transmission error as well. Once again new concepts are introduced for the model complexity and the finite element analysis is conducted by Abaqus.

5.2. Finite Element Method

5.2.1. Model Creation

According to the test stand configuration, two shafts are additionally created and imported from the CAD program, Inventor. They are merged to the presenting helical gear model as shown in Figure 39. The dimensions of shafts are referred to as the parts in the test rig. However, the details such as the spline or holes on shafts are left out due to the mesh complexity. As the educational version of Abaqus has limits to node numbers, the total number of nodes cannot exceed more than 250,000. Later, the gear teeth have taken most of the mesh assignment. Materials are assigned in the same way as previous models.

5.2.2. Interaction and Load

Basically, an object has six degrees of freedom. Three translational movements along the x, y and z axis and three rotation about x, y, and z-axis. These degrees of freedom should be limited by certain components that place in the test stand configuration. The places where the ball bearings and the needle bearings locate are assigned corresponding constraints. In Figure 40 [8], right below the Abaqus CAD model, the part of the test rig construction can be found in a similar angle to help better understanding. The constraint on the ball bearings (in red circles) is to limit all the motions except the revolution along the axis of rotation. On the parts where the needle bearings (in green circles) are assembled, not only the rotation on the axis but also the translation along the rotation axis are also accepted. Yellow cross marks are the reference points and it becomes the central region of each constraint or applied load and angular velocity. Also, to ensure that the system is coupled with the rest of the parts of the test stand, the ends of shafts remain as rigid bodies. All of the constraints work on specific surfaces where the components are assembled. The partitions on the shafts are separated to make this possible.

This complex model as well as the helical gear model has the same applied loads. But this time the regions where the angular velocity and the moment are applied locate at the points where the primary shafts are coupled since the driving motor and applied torque point located on the end of the primary shafts (to the right bottom side in the figures). These two shafts on the same axis are coupled with the help of clutches. Like the helical gear model in the previous chapter, two analyses are done at two different

applied angular velocity. One is assigned with 1250rpm and the other one is assigned with 2000rpm to check the transmission error in different input speeds. Ramp-up delay should be added depending on the amount of input angular velocity so that the speed would gradually increase. It prevents the gear teeth from having excessive deformation and helps to minimize the rebound problem which was mentioned in the trial and error section.

On a dynamic implicit model for static TE analysis, only 60 rpm of speed is assigned on the input shaft to minimize the effect by dynamic motions of components. As it is under slow condition, no ramp-up delay has been used. Due to the low speed, it may cause different influences on the lubrication of gear meshing. Thus, different friction coefficient should be used for the contact property.

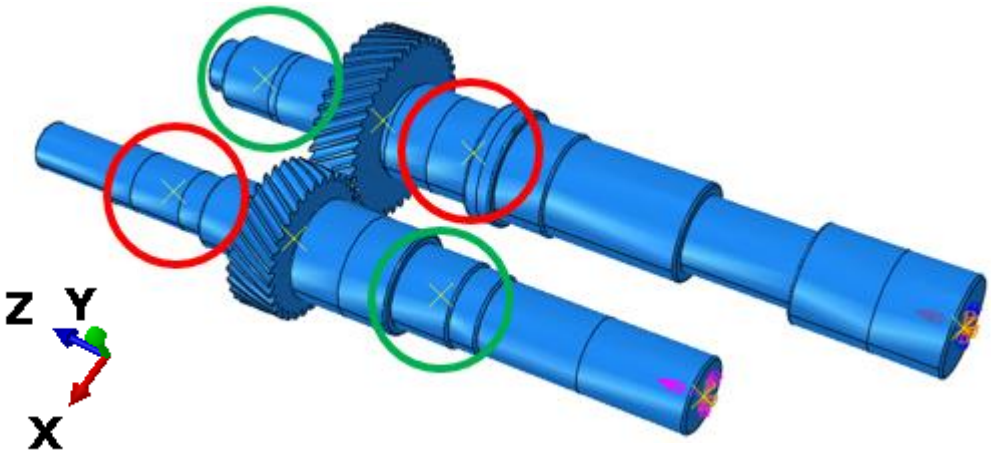

Figure 39. Assembly model of complex helical gear model

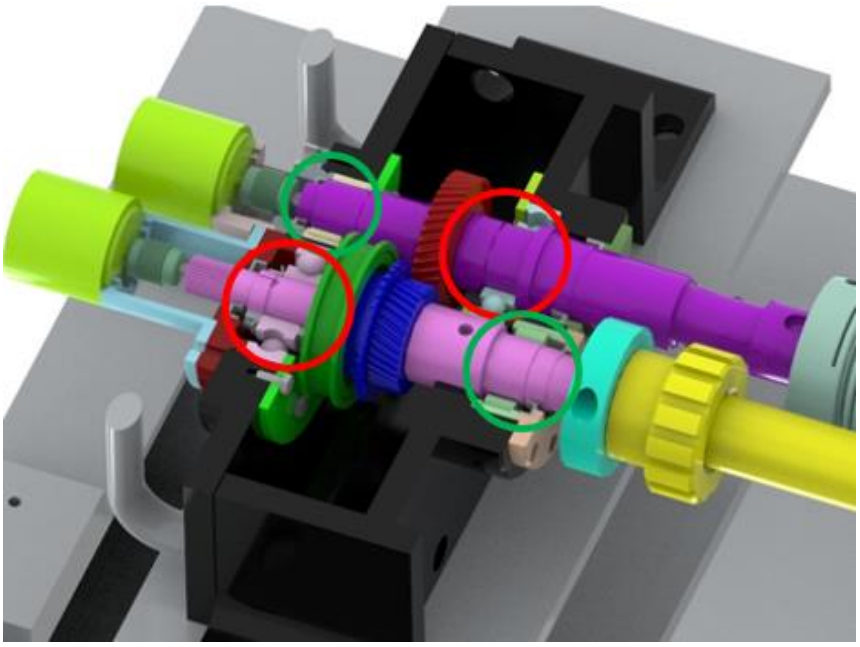

Figure 40. Test rig configuration [8]

5.2.3. Mesh and Step

The educational version of Abaqus has a limited number of nodes. Hence, the mesh is focused on the gear components and the shafts take only rough mesh not to go beyond its limits. The explicit C3D8R element is assigned for the whole model. As the problems have mentioned in the "Trial and Error" section, hourglass control and distortion control in mesh have to be turned on. The total number of nodes on the input parts is 96875 and that of the output parts is 110459.

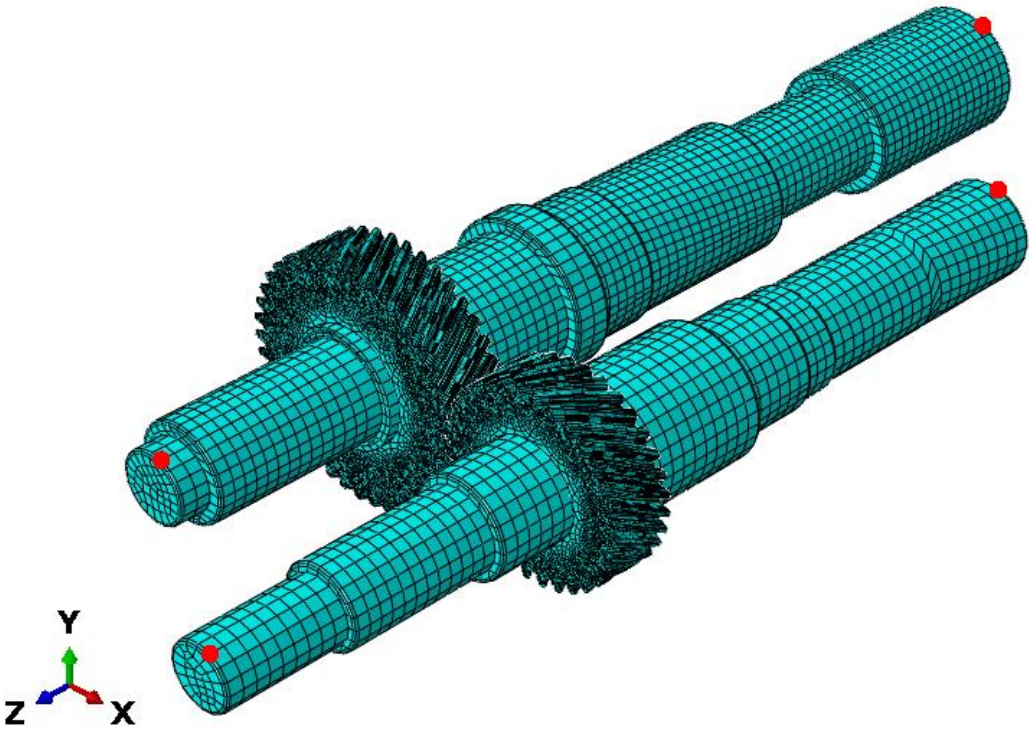

Figure 41. Generated mesh on complex model and selected node set

Like the description in chapters before, Abaqus can provide the required outputs of selected nodes. If the other parameters without necessity are not called for the result, the file size becomes smaller and it eases the data processing. Thus, it is more desirable to pick several nodes in concern instead of requesting information from the whole model to reduce the analysis output. To do so, it should be firstly ensured that the models operate correctly. It can be done by checking stress distribution for a few milliseconds. In this chapter, the choice of nodes is a bit different from the previous ones that contain no shafts. Two nodes where the speed sensors locate are chosen corresponding to the test rig instead of those on bores of gears. Those are placed on the left bottom side of the figure. In addition, extra two nodes on clutch sides are selected as well to compare the transmission errors on both ends of the shafts. Those are placed on the right top side of the figure. This set of nodes is the target of output and further data processing. The comparison between the transmission errors on each shaft end may demonstrate the effect on transmission error, especially along the same shaft. The velocity parameter of the selected nodes is chosen to be derived. In Figure 41 above, the mesh formation of the model is presented. Also, specific nodes for output

request can be found with red dots on both sides of shafts. They are located in the outer diameters of the shaft ends.

5.3. Result

5.3.1. Abaqus

To see the result of finite element analysis in Abaqus, Figure 42 is presented. The translational velocity is graphically shown in the figure. It shows velocity distribution on the set model's geometry and its corresponding unit is mm/s by the Abaqus. Owing to the transmission error, its effect reaches the center of gears and the shafts. The amount of the velocity on each part of the gears differs according to the gear meshing timing. As it is obvious, the velocity is larger in the area which has larger thickness.

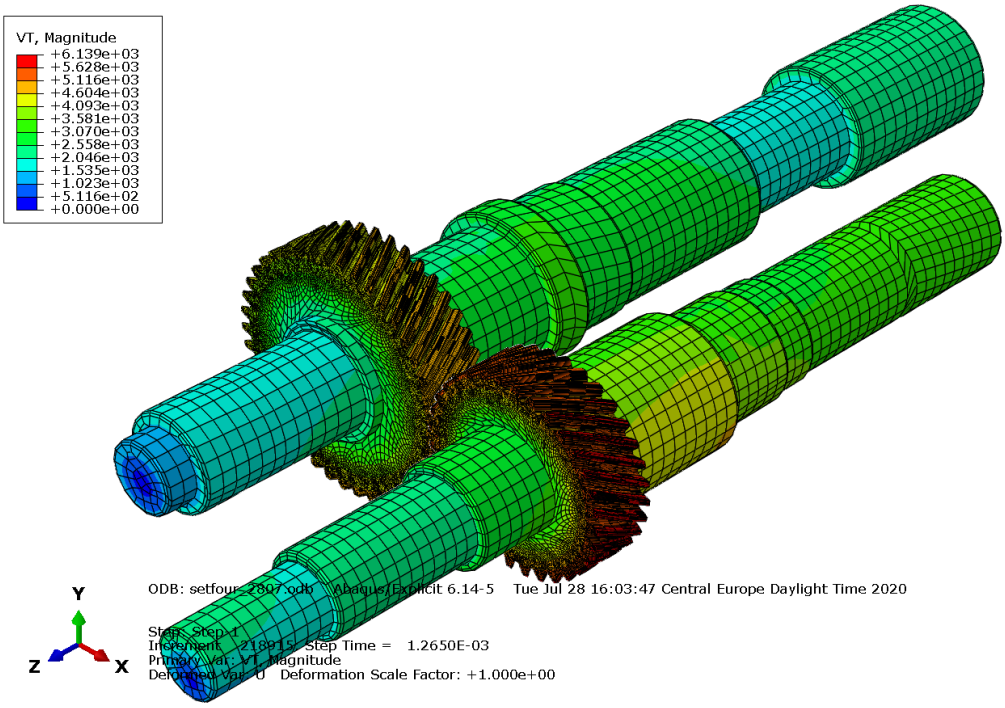

Figure 42. Velocity distribution on complex model

The following three graphs show the time versus velocity plot by Abaqus. As it can be seen in those plots, models of Figure 43 and 44 have been conducted under the angular velocity of 1250 rpm and 2000rpm respectively. Next of them, the input angular velocity of the model in Figure 45 is only 60rpm for the analysis under the static condition. Each plot presents four nodes on the sensor sides and those on the clutch sides of the input and the output shaft. The locations of the nodes are written in the legend and can be distinguishable by colors.

Analyses are continued until the behavior of the model becomes stabilized. In common with the helical gear model, the initial velocity is clearly seen with a constant value. Other factors are oscillating due to the initial condition. In the static model, the fluctuation of the nodes on each shaft is little after the first impact at the beginning of the simulation. Only some small oscillation is visible and their values are nearly

constant. This data consisting of time, node velocities on the input shaft, and node velocities on the output shaft is exported as a form of Excel sheet to NI DIAdem for TE calculation.

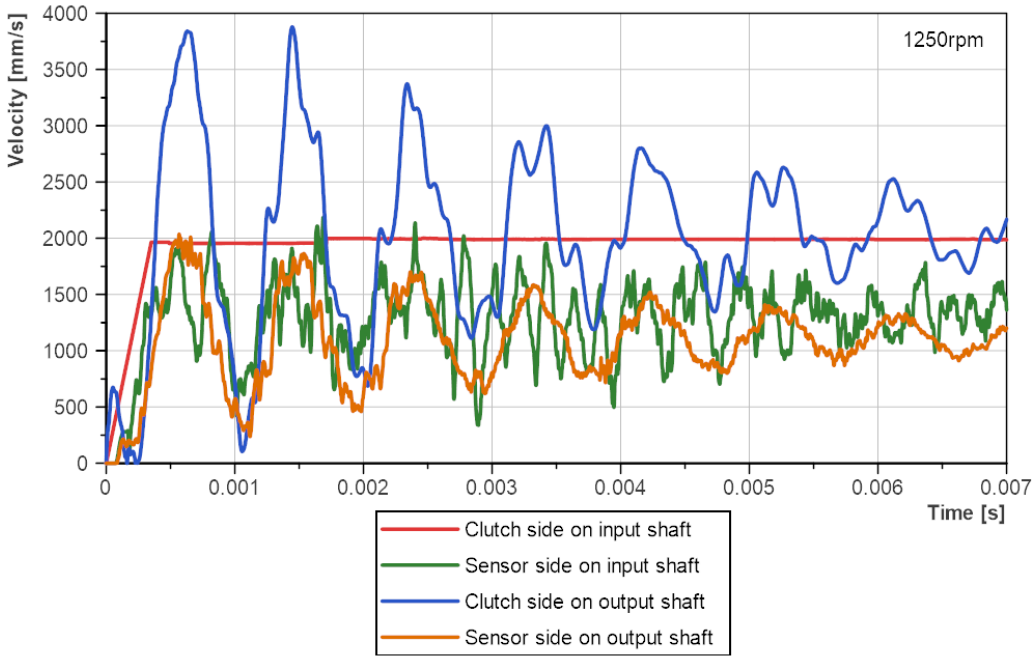

Figure 43. Velocity of nodes at 1250rpm

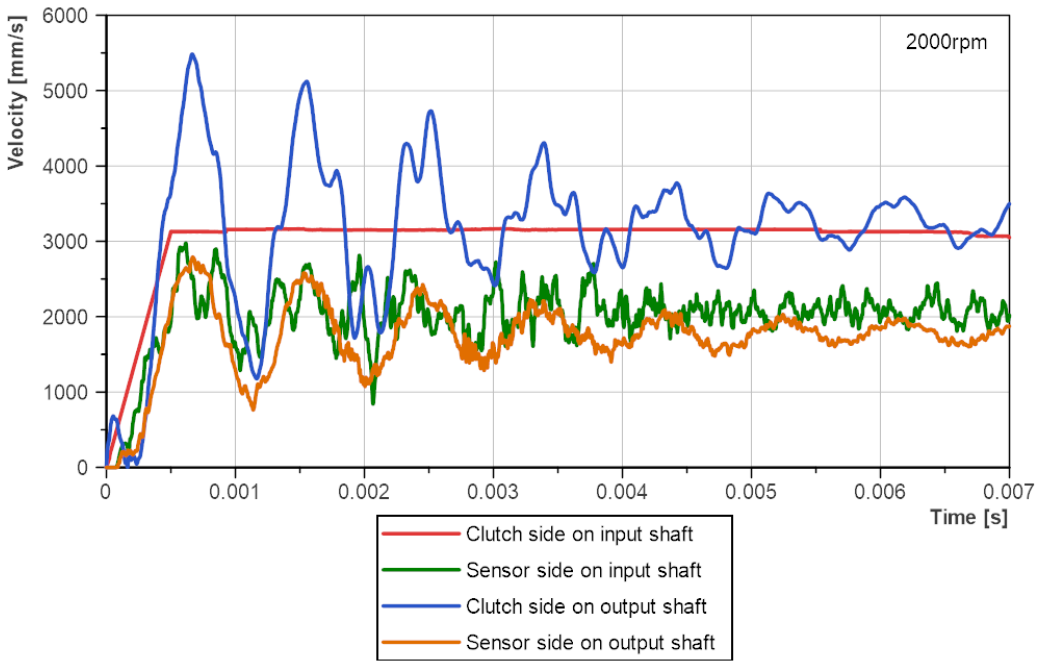

Figure 44. Velocity of nodes at 2000rpm

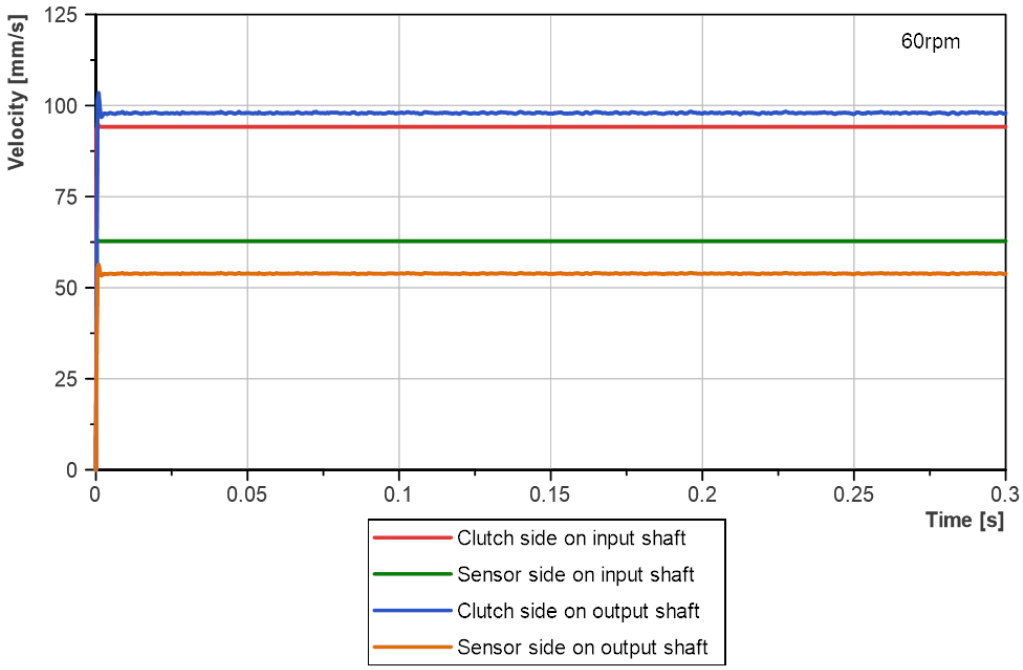

Figure 45. Velocity of nodes at 60rpm

5.3.2. NI DIAdem

Now the data processing according to TE calculation is to be done with NI DIAdem software just like in previous chapters. Before that, some of the variables in Equation 34 should be substituted with other variables because the nodes as output variables are not assigned on the bores of gears anymore. Instead of the radius and velocity on nodes, the equations can be modified by using the dimension and velocity of shafts on both ends. The following two equations state the way of TE calculation on clutch and sensor sides.

$$TE \text{ on clutch side} \qquad TE_s = \frac{r_1}{r_{c1}} \int v_{c1}\ dt - \frac{r_2}{r_{c2}} \int v_{c2}\ dt\ [mm] \qquad 39$$

$$TE \text{ on sensor side} \qquad TE_s = \frac{r_1}{r_{s1}} \int v_{s1}\ dt - \frac{r_2}{r_{s2}} \int v_{s2}\ dt\ [mm] \qquad 40$$

$\boldsymbol{v_c}$ is velocity on the clutch side. $\boldsymbol{v_s}$ is velocity on the sensor side. $\boldsymbol{r_c}$ is the radius of the clutch side shaft and $\boldsymbol{r_s}$ is that of sensor side shaft. Numbers 1 and 2 indicate the input shaft and the output shaft respectively. DIAdem script which is written based on these equations is shown in Figure 46. The multiplied constants are the ratio of the pitch radius and the shaft radius on the clutch side or the sensor side.

```
'Set model TE (clutch side)'
Set ChnResult = ChnIntegrate("[26]/Time","[26]/Input_c","[26]/alpha1","TrapezoidalRule",0,0,0)
Set ChnResult = ChnIntegrate("[26]/Time","[26]/Output_c","[26]/alpha2","TrapezoidalRule",0,0,0)
Set ChnResult = ChnLinScale("[23]/alpha1","[23]/L1",(28.3003/15),0)
Set ChnResult = ChnLinScale("[23]/alpha2","[23]/L2",(36.25975/20),0)
Set ChnResult = ChnSub("[26]/L1","[26]/L2","[26]/TE_c")
'Set model TE (sensor side)'
Set ChnResult = ChnIntegrate("[26]/Time","[26]/Input_s","[26]/alpha3","TrapezoidalRule",0,0,0)
Set ChnResult = ChnIntegrate("[26]/Time","[26]/Output_s","[26]/alpha4","TrapezoidalRule",0,0,0)
Set ChnResult = ChnLinScale("[26]/alpha3","[26]/L3",(28.3003/10),0)
Set ChnResult = ChnLinScale("[26]/alpha4","[26]/L4",(36.25975/11),0)
Set ChnResult = ChnSub("[26]/L3","[26]/L4","[26]/TE_s")
```

Figure 46. TE calculation script for set model

Finally, the transmission error is obtained for all different speeds and plotted below on both sides where the clutches locate and where the sensors locate. Figures 47, 48, and 49 show TE at 1250rpm, 2000rpm, and 60rpm respectively.

As it is seen in Figure 47 and 48, there is a small phase shift between the waves of both sides. The wave of transmission error on the sensor lags a little bit behind that on the clutch. It is an influence of not perfectly rigid shaft since the deflection of the parts should be transmitted to the other end of the shaft. When it comes to the amplitude of TE, the sensor side has a smaller value than the clutch side. It can be due to the reason that clutch sides have the points where the initial angular velocity and torque are applied. As the loads are close to the nodes on the clutch side, they are under higher stress than the other side. To compare the results on two different angular velocities, the transmission error amplitude at 2000rpm is larger than that at 1250rpm in the beginning. Then the amplitude of 2000rpm repeats to fluctuate at a similar level and a larger level. Seemingly, 2000rpm has more undulation and less stabilizing tendency. It cannot be generally stated that the higher speed causes the larger TE since the analyses are conducted under only two different speeds, not under fully spread speed bend. Besides, there can be more mutual interaction among additionally assembled parts and input parameters. This can be a recommended future work to figure out the impact of multiple factors on the transmission error.

The static transmission error in Figure 49 is caused by the imperfect gear geometry and stiffness of the components as the dynamic factors are crossed out by the low input velocity. The eccentricity or the assembly error cannot be considered as it is a precise computational model. In the slow model, the evident phase shift between the different sides of shafts barely occurs. The fluctuation still exists but the amplitude is much smaller than that of TE under the dynamic condition. Its inclination is still clearer than that of dynamic models since the undulation by dynamic transient response is little.

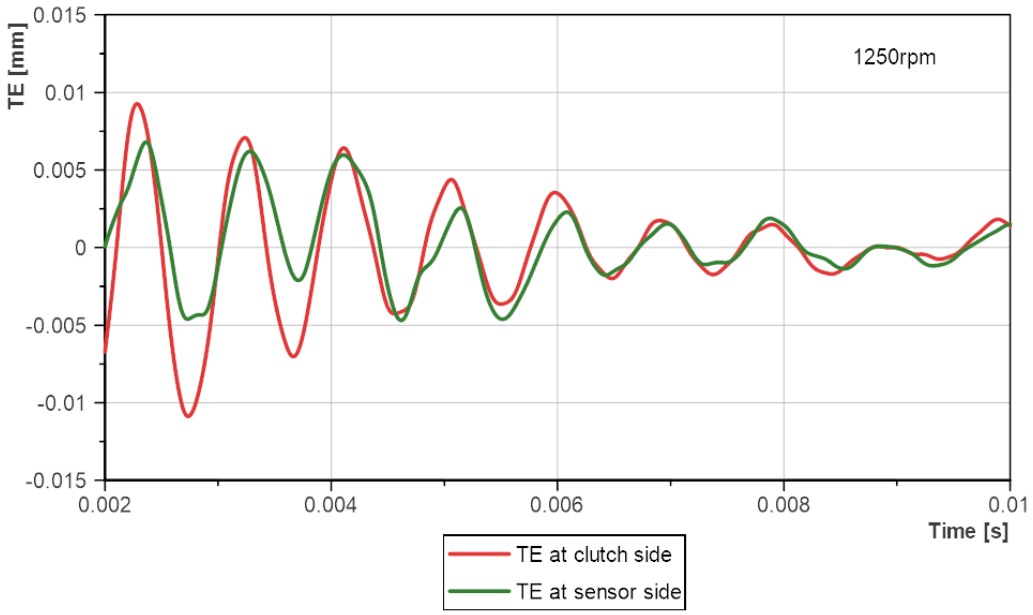

Figure 47. TE of complex model on clutch and sensor side at 1250rpm

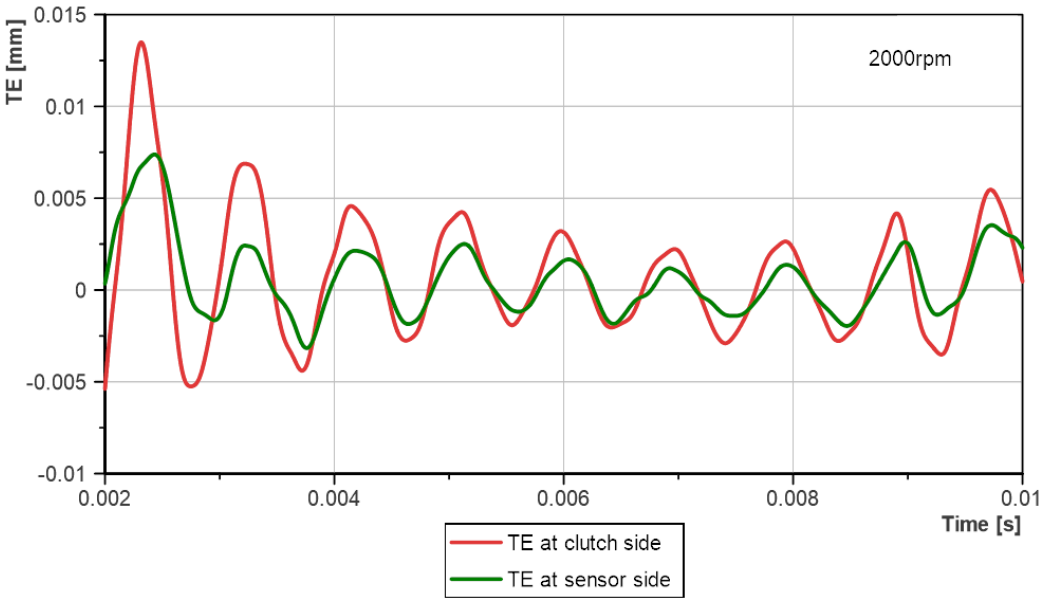

Figure 48. TE of complex model on clutch and sensor side at 2000rpm

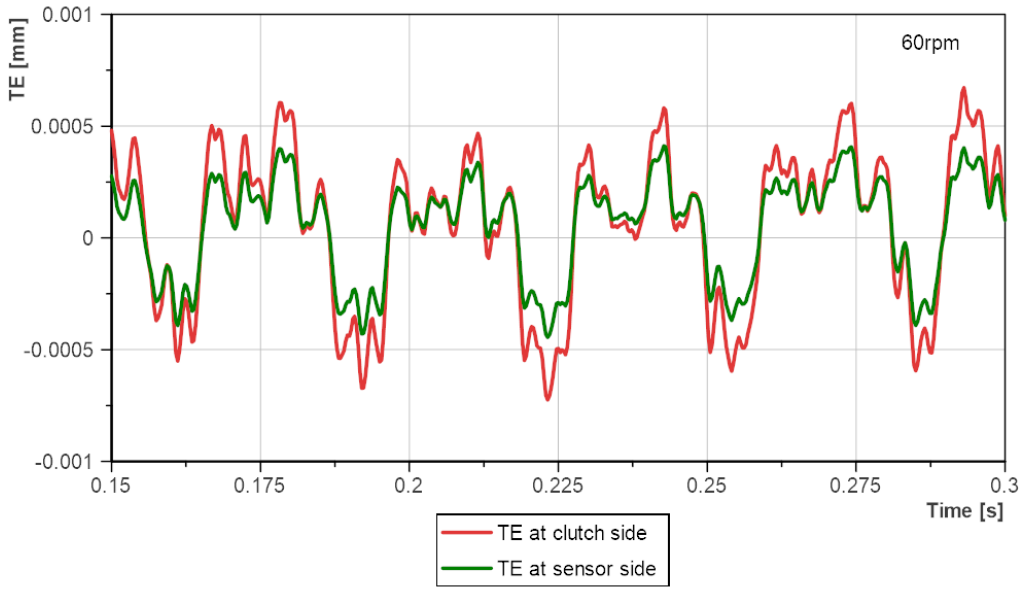

Figure 49. TE of complex model on clutch and sensor side at 60rpm

To confirm the TE behaviors, these graphs have to be transformed into a frequency domain accordingly using FFT. Frequency versus amplitude peak graphs give clues about gear meshing frequency at different gear speeds. It can help to check whether the transmission error corresponds to the gear mesh or not. Following Figures 50, 51, and 52 are the results after FFT with the angular velocity of 1250rpm, 2000rpm, and 60rpm respectively. A few gear mesh frequencies are marked on each plot.

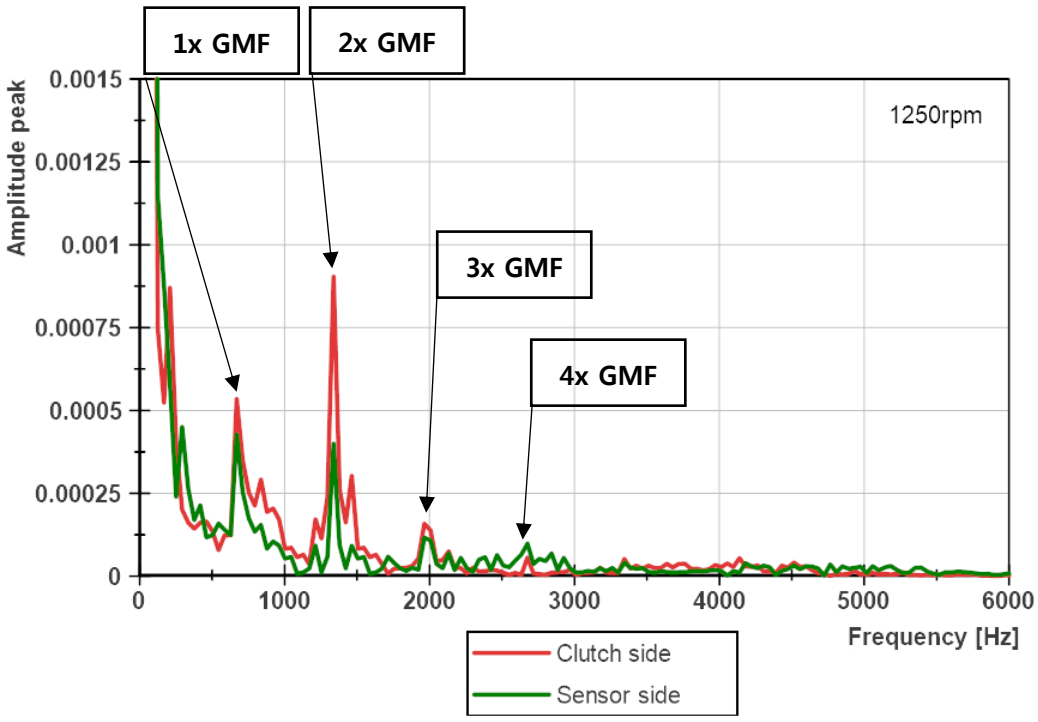

Figure 50. Frequency domain of complex model at 1250rpm

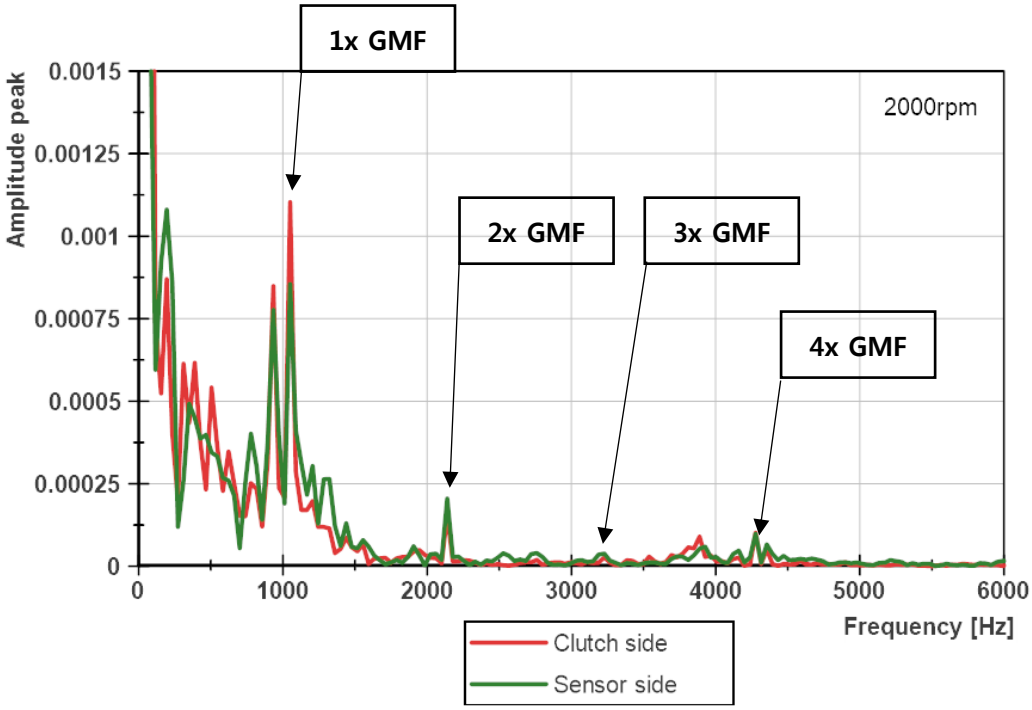

Figure 51. Frequency domain of complex model at 2000rpm

As discussed in the previous chapter, the frequency band in the dynamic analysis is much wider compared to the obtained number of samples to harmonize the sampling frequency to the encoders in the test rig. This makes the frequency-domain value become sparsely. The amplitude peaks at exact gear mesh frequency cannot be read on this account, but the close-by values are obtained.

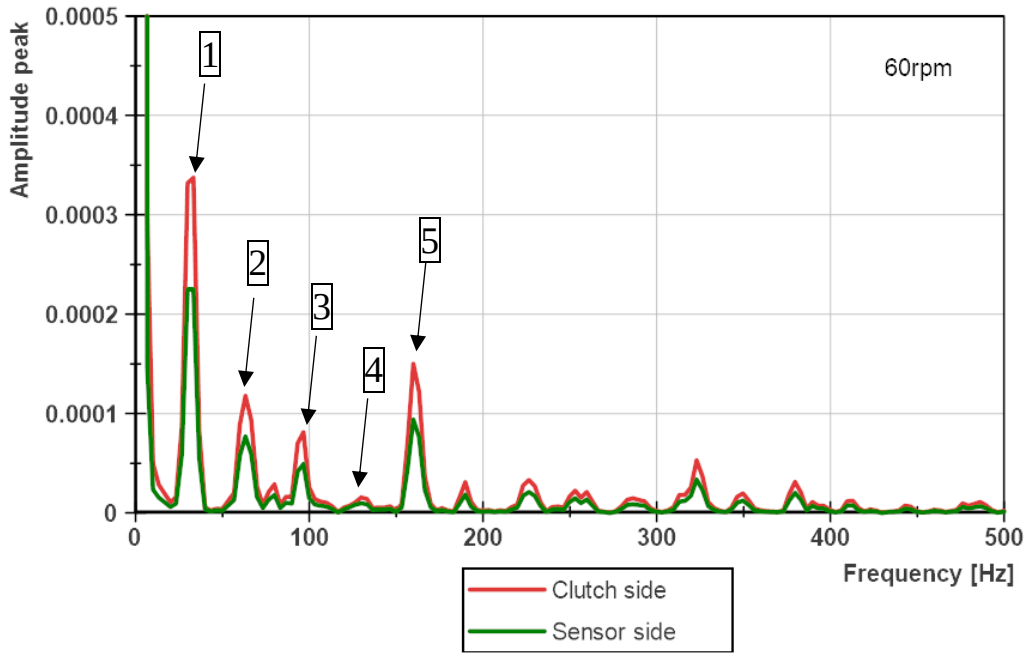

Figure 52. Frequency domain of complex model at 60rpm

The frequency-domain of static transmission error has a clearer tendency to have high peaks on gear mesh frequency. The first five GMFs are indicated by numbers. The first GMF is 32Hz and with an interval of this frequency, the other peaks are distributed. Its amplitude diminishes in the high-frequency zone as any other result. The highest peak before the first gear meshing is caused by the initial excitation.

5.4. Conclusion

Transmission error in high speed is influenced not only by the gear teeth deformation but also by dynamic behaviors by other components. This chapter has aimed to clarify the mutual interaction among parts. A new complex helical gear model has been created with input and output shafts which are connected to other transmission systems. To increase the similarity to the test stand, several more boundary conditions and constraints are added. On the locations where the bearings are, certain degrees of freedom are assigned. Rigid bodies for clutch coupling, corresponding restrictions of movement for ball bearings and needle bearings are defined on the shafts. Dynamic TE on different sides of shafts is calculated under the various speeds of 1250rpm and 2000rpm. By the TE result with an input velocity of 60rpm, static transmission error has been analyzed as well. To verify the results, frequency versus amplitude peak graphs are used to check the conformity of the system by reading the peaks in GMFs.

6. Comparative Analysis

At last, the final results of the complex helical gear model and those by the experimental test bench are compared and the difference is contemplated. The correlation between measurement by the test rig and the simulation by Abaqus for the gear mesh model is carried out under the same loaded condition. The result of the experiment is by the incremental rotary encoders which are located in the sensor side of shafts in the finite element model, so only the output of this side from Abaqus will be expressed this time, excluding the output of the clutch side.

In the following figures, transmission error by the empirical method and that by FEM can be found at different speeds. To observe their behaviors during the rotation, the angle parameter is used on the x-axis. The ranges and phases are adjusted to compare the tendency of each TE.

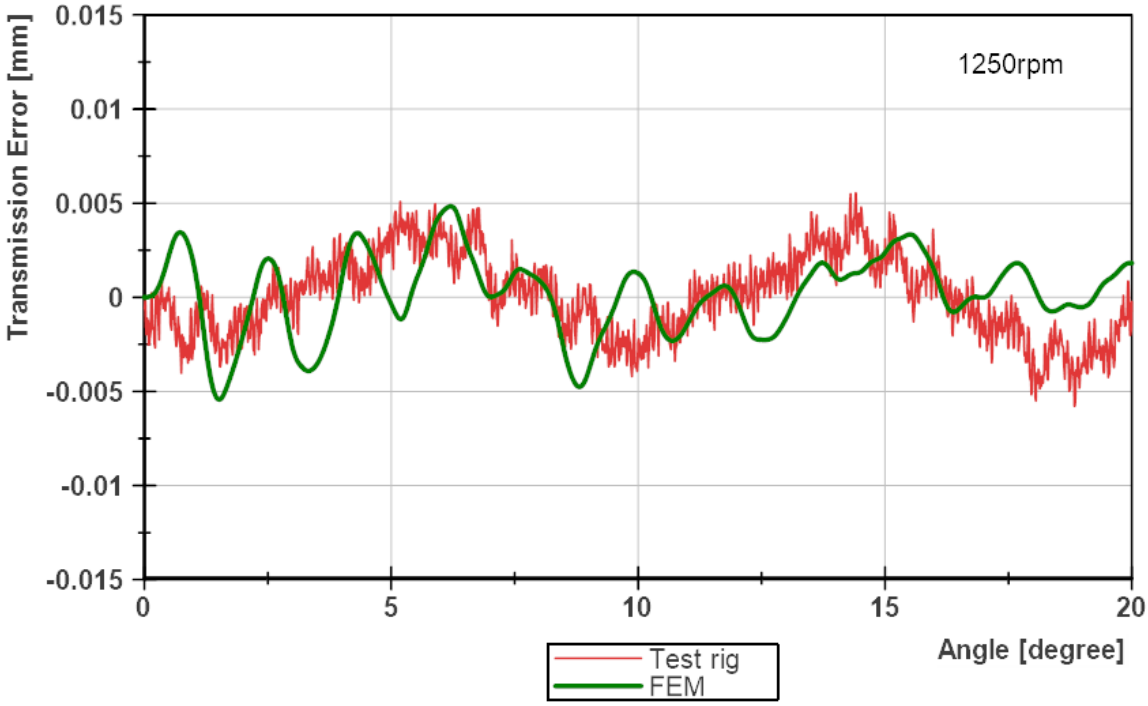

Figure 53. Measured TE and analyzed TE at 1250rpm

There are serious fluctuations of each result line of dynamic simulations and this phenomenon implicates the excitations in gear meshing as frequency domain graphs have been presented. The undulation is typical dynamic transient response. In Figure 53, the transmission error measured by the test rig and analyzed by the finite element method is shown. Both of the TEs have their tendencies which oscillate with a similar period. Figure 54 shows the result at 2000rpm and the difference seems noticeable. The regular patterns are rarely seen on both TEs during the same rotational angle as 1250rpm. The high-frequency fluctuation in the test rig is possibly from the electrical noise in the circuit. The irregular difference between the two speeds can attribute to the components under vibrations

At the speed of 60rpm, it has been found out that the test stand is not capable to catch an appropriate outcome for the static transmission error. The vibrations of other tested components are more dominant so that the deflection of teeth and the effect from the tooth profile are not visible.

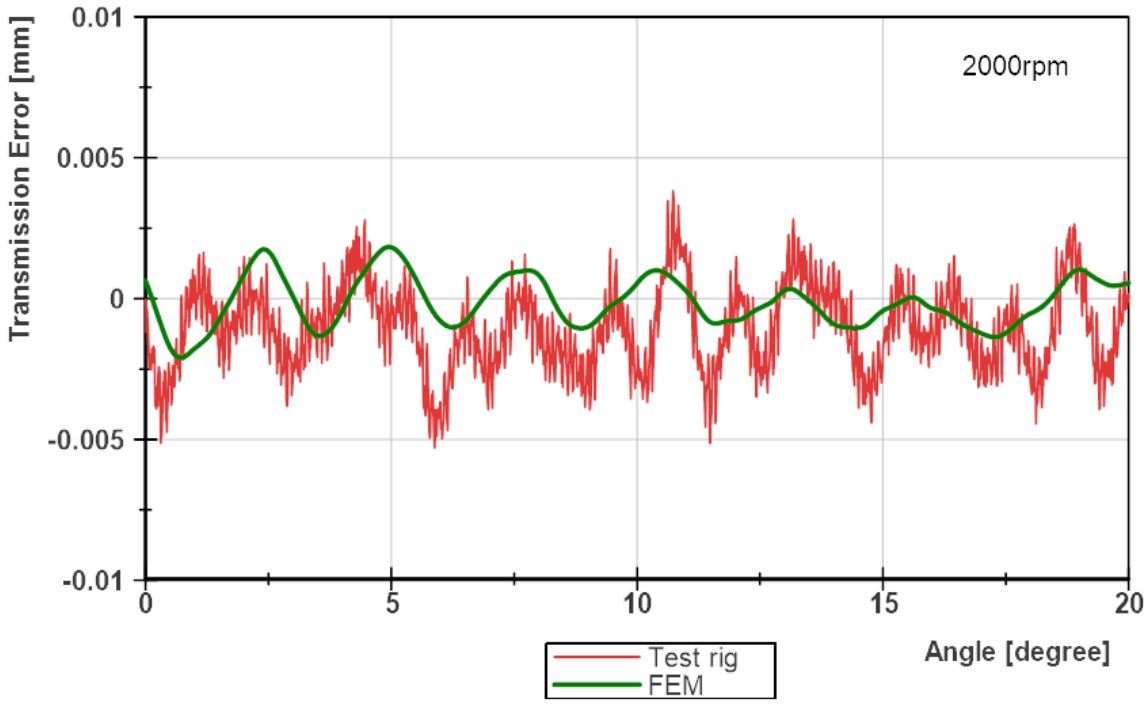

Figure 54. Measured TE and analyzed TE at 2000rpm

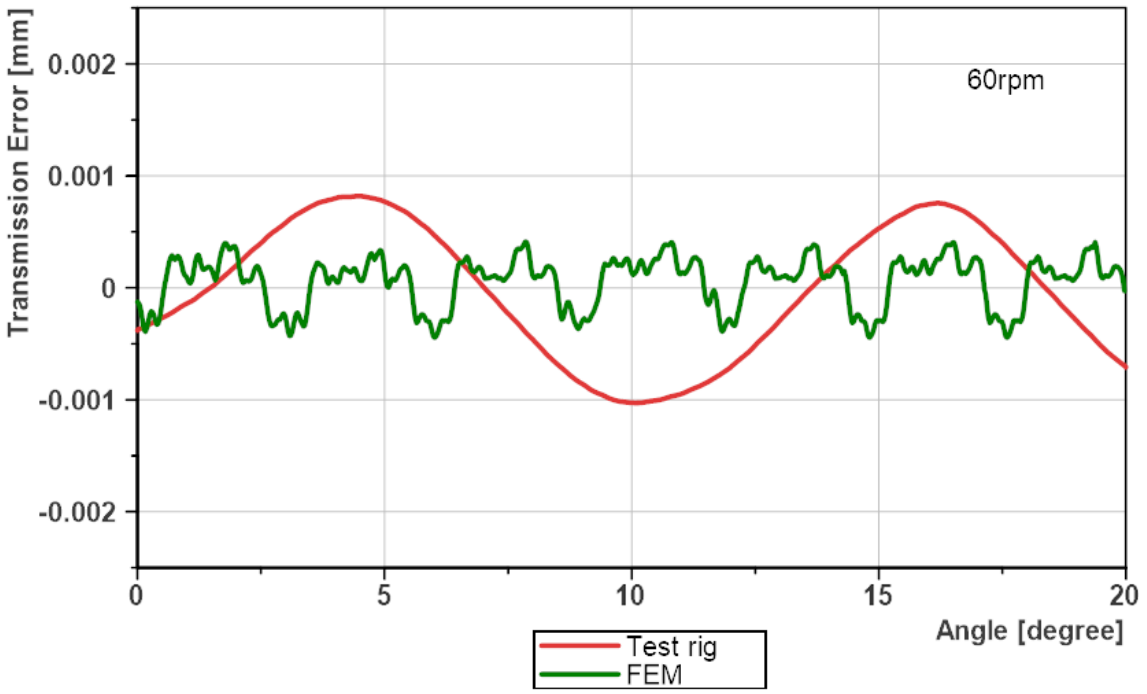

Figure 55. Measured TE and analyzed TE at 60rpm

Now the frequency domain graphs are compared in Figures 56 and 57. In both cases, high peaks appear generally at the gear mesh frequency. This means that the systems are correlated to the gear mesh timing. Other peaks that are placed out of the GMF are due to the natural frequencies of the system and the impact by the initial excitation. As the sampling numbers are greater in the test rig, the result seems denser than that by the finite element method.

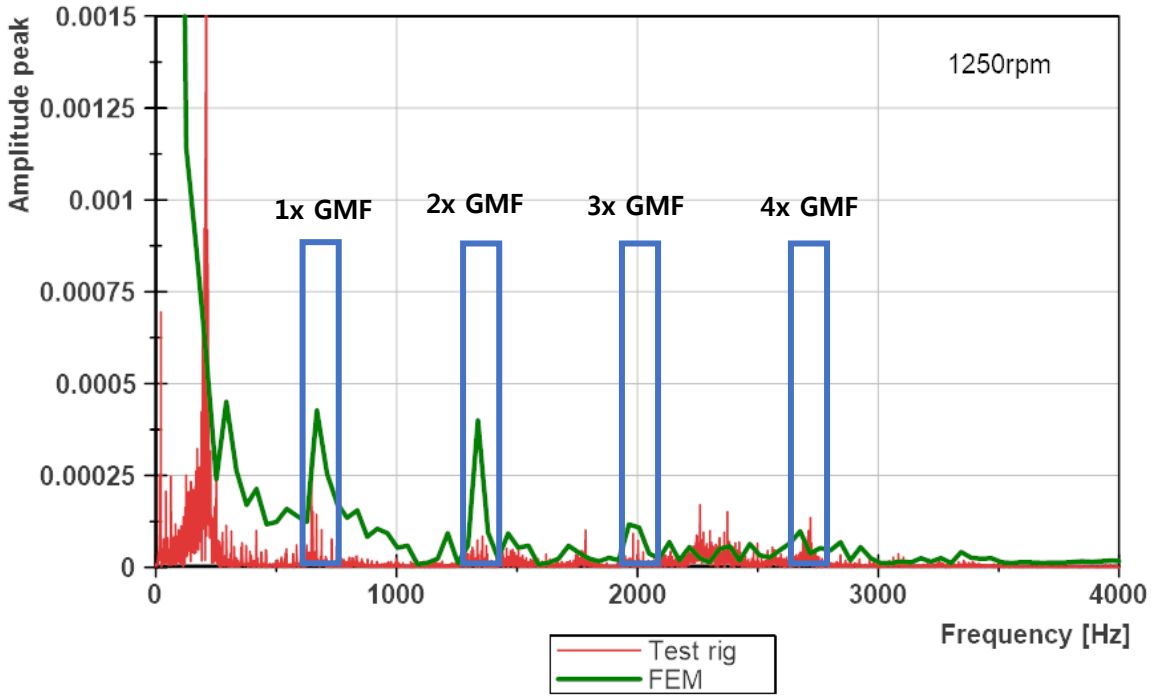

Figure 56. Frequency domain of test rig and FEM at 1250rpm

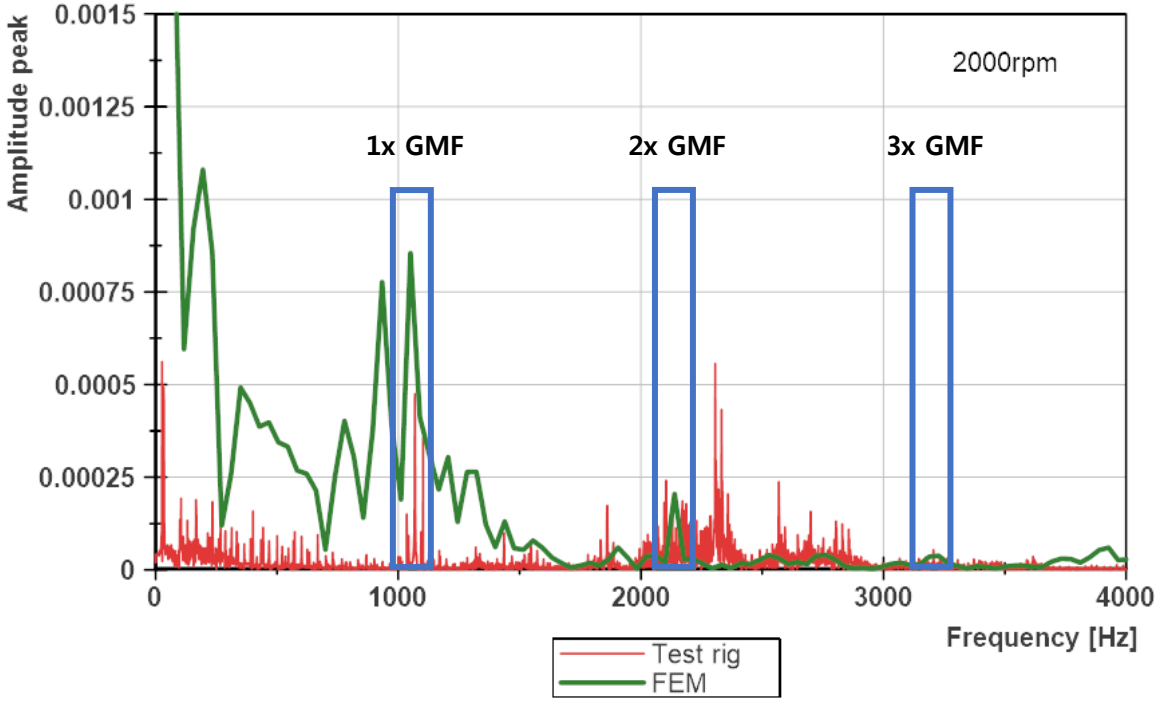

Figure 57. Frequency domain of test rig and FEM at 2000rpm

7. Conclusion

7.1. Summary

This paper contains three models of the geared transmission. The initial approach starts with a bare pair of two spur gears. As the simulation is mainly run by Abaqus, which was an unaccustomed work for the author, preparation and possession of basic knowledge were needed. By a quite simple model like this, it was possible to conduct a useful investigation of the dynamics of the transmission before dealing with more complex models. By adding advanced parameters like extra features including input and output shafts on the analyzed model, and by applying more complex constraints and boundary conditions, improved models closer to the reality were created. These have allowed that the result which may show more details like the test stand could be derived.

Even though gear dynamics has been studied for decades, few studies present the complex gear train system that contains deformable shafts and bearings constraints. Some have ended up with simplified modeling of gear mesh interface or two-dimensional models which neglect out of plane behavior. This study attempts to fill this gap with a general finite element formulation and to get closer to the complex gearbox dynamic analyses.

The data from the test rig and that from the finite element method have been compared. The results may have significant differences because of many reasons. One of the main reasons can be from the gear design. Even though most of the parameters are taken into account, the gear models still do not reflect the real ones. Mechanical tolerances by the manufacturers, defects during the assembly process, and wear properties remain unknown. Flexible input and output shafts are simplified due to the limit to the number of mesh as well. The accurate material property of real gears and shafts remains unknown as well. When it comes to the transmission error, only a few small factors may significantly vary the result, since the unit of the output is just a few micrometers. Also, several suppositions were made such as temperature effect on the deformable material. Still, some of the transmission parts are absent compared to the test rig as the model consists of only two shafts and a pair of gears that are mutually interacting.

It is also necessary to mention that the finite element method in this research is only based on the computational method, so the conclusions and discussions may not be very accurate in reality. There is a further significance above all of these factors which are not considered. The research strategy does not completely cover all complicated dynamic responses caused by various external and internal excitations in real gear meshing. This study is hoped to discuss basic typical phenomena that are derived from static and dynamic responses. It is also hoped to help to understand theoretical transmission error and introducing the concept of methodologies for advanced researches.

At last, this thesis is hoped that other new researchers who may work on similar fields with similar methods would refer to some of the items that can help their study. When it comes to the research, the majority of the people must agree that a few sentences in books or theses can be a great help to set the direction and to build a solid base of the work. The author wishes that this thesis can be small support to somebody who dreams to be an engineer as well.

7.2. Future work

The major recommendations that can be made for future work in this field of gear research are mainly based on the continuance of the current approach. The introduced finite element models can be further developed to allow for more degrees of freedom, in order to achieve a more complex representation of the realistic gear system. Finite element simulations that have been carried out in this thesis include only a few elements from the total gear set. In a future study, this could be expanded to include a 3-D model with other components and more complete boundary conditions and interactions that can cover characteristics of materials, temperature variants that can bring more complex mutuality among parts.

Besides, new parameters that affect the transmission system can be introduced. In an actual gear transmission, misalignments of the components, imperfect helix shape, and irregular wears on gear teeth are existent. Some parameters change by time and the transmission error can enter upon a new phase due to these reasons. Most of the studies assume that the operation takes place under ideal conditions without consideration of changes according to the time of performance. However, these factors need to be dealt with to know the transmission error during the overall lifespan of the mechanical transmission.

Also, the variation of the initial load and speed can be extended. This thesis has covered only a few speeds at the same torque and it is hard to conclude the tendency of the model in the whole operation range. According to the operating conditions of gearboxes, loaded torques and speeds can be matched to obtain the transmission error under the appropriate range of the engine. This may also help to predict the characteristics of TE along with gear whining or vibration problem of the vehicle.

Finally, the finite element analysis can be optimized to reduce the calculation time. As it is common for FEM, it takes extreme computational time depending on the quality of analysis and the number of mesh elements. In this study as well, it was a tiresome work to run the model and obtain the result repeatedly because the models could not be always flawless. For instance, one simulation had taken longer than two weeks to obtain 0.03 seconds of the result. Sometimes the total analysis had been suspended due to the server issue. It is uneasy to utilize the finite element method without the help of a high-performing computer and a stable server connection. Using a modal reduced model can allow to drastically reduce the computational time compared to transient FE simulations.

As mentioned in the chapter “Review of Previous Research”, it shows that there are many potential ways to study the transmission error. And still, not all the possibilities are considered to discover the impacts on the TE under possible circumstances. Solutions are being improved and optimized by the researchers all around the world and the future works are expected to contribute to accumulating knowledge about the transmission error.

8. List of Figures

9. List of Tables

10. References and Literature

[1] Lin, T., He, Z.: Analytical method for coupled transmission error of helical gear system with machining errors, assembly errors and tooth modifications, Mechanical Systems and Signal Processing, 91 (2017), pp. 167-182, DOI: 10.1016/j.ymssp.2017.01.005

[2] Nikolic, V., Dolicanin, C., Dimitrijevic, D.: Dynamic Model for the stress and strain state analysis of a spur gear transmission, Strojniški vestnik - Journal of Mechanical Engineering, 58 (2012), pp. 56-67, DOI: 10.5545/sv-jme.2009.128

[3] Korde, A. and Mahendraker, V.: Drive noise reduction by predicting mesh transmission error and micro geometry optimization, SAE Paper, (2009), DOI: 10.4271/2009-26-0052

[4] Tharmakulasingam, R. : Transmission error in spur gears: static and dynamic finite-element modeling and design optimization, Brunel University, (2009) http://bura.brunel.ac.uk/handle/2438/5100

[5] Palermo, A., Mundo,D., Hadjit, R. and Desmet, W.: Multibody element for spur and helical gear meshing based on detailed three-dimensional contact calculations, Mechanism and Machine Theory, 62 (2013), pp.13-30, DOI: 10.1016/j.mechmachtheory.2012.11.006

[6] Neusser, Z., Sopouch, M., Schaffner, T., Priebsch, H.: Multi-body Dynamics Based Gear Mesh Models for Prediction of Gear Dynamics and Transmission Error, SAE Technical Paper, (2010), DOI: 10.4271/2010-01-0897

[7] Kučera, P., Píštěk, V., Prokop, A., Řehák, K.: Transmission error analysis for heavy-duty gearbox, Brno University of Technology, (2018), DOI: 10.21595/vp.2018.19919

[8] Kazda, L., Milacek, O.: Transmission test rig, Czech Technical University in Prague AutoSympo 2018

[9] SICK Incremental encoder DFS60B-S1PL10000, SICK, [Online], [Retrieved 11.07.2020] https://www.sick.com/cz/en/encoders/incremental-encoders/dfs60/dfs60b-s1pl10000/p/p293762?fbclid=IwAR1EcNKucveOsftGw2p2JzKwtkprPogtgwe48qZY5ZLzCaLZpV-sSqEVwMs

[10] Fourier transform, Isaac's science blog, [Online], [Retrieved 12.06.2020] https://isaacscienceblog.com/2017/08/13/fourier-transform/

[11] Jančík, L.: Machine Elements and Mechanisms I (study texts), CTU, Prague, (2006)

[12] Gear nomenclature, Transmisi, [Online], [Retrieved 03.07.2020] http://transmisi.blogspot.com/2009/05/gear-nomenclature.html

[13] Step definition with stable time increment, Abaqus documentation – MIT, [Online], [Retrived 15.07.2020] http://194.167.201.93/English/SIMACAEGSARefMap/simagsa-c-ovwdefinition.htm

[14] Kim, M., Kim, Y. : Nonlinear Finite Element Analysis for Mooring Chain Considering OPB/IPB, Journal of Ocean Engineering and Technology, 31 (2017), pp. 299-307, DOI: 10.26748/KSOE.2017.08.31.4.299

[15] Contact pressure-overclosure relationships, Abaqus documentation - MIT, [Online], [Retrieved 02.07.2020] https://abaqus-docs.mit.edu/2017/English/SIMACAEITNRefMap/simaitn-c-normalinteraction.htm

[16] Integration points for output, Abaqus Analysis User's Manual, [Online], [Retrieved 13.07.2020] http://130.149.89.49:2080/v6.9/books/usb/default.htm?startat=pt06ch24s01ael02.html

[17] Hourglassing and shear locking, Optimec consultants, [Online], [Retrieved 13.07.2020] http://optimec.ca/news/how-to-model-bending-and-bending-dominated-problems-in-abaqus/

[18] Chung, C., Steyer, G., Abe, T., Clapper, M. et al.: Gear Noise Reduction through Transmission Error Control and Gear Blank Dynamic Tuning, SAE Technical Paper 1999-01-1766, (1999), DOI: 10.4271/1999-01-1766.

[19] Ma, J., Li, C., Cui, L.: Transmission Error Analysis and Disturbance Optimization of Two-Stage Spur Gear Space Driven Mechanism with Large Inertia Load, Hindawi-Shock and Vibration, (2018), DOI: 10.1155/2018/6863176

[20] Malviya, D., Sharma, P. K.: Transmission Error in Gear, International Journal Of Modern Engineering Research, 4 (2014), ISSN: 2249–6645

[21] Naunheimer, H., Bertsche, B., Ryborz, J., Novak, W.: Automotive Transmissions, Springer, (2010), DOI: 10.1007/978-3-642-16214-5

11. Annexures

11.1. Input gear specification

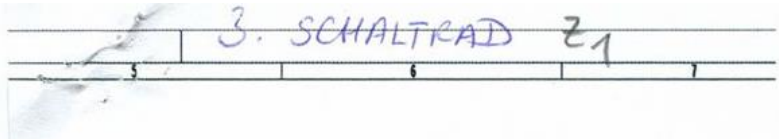

Teilnummer o.Z.	02T 311 131 AS		
Uebersetzung	41:32		
Kennzeichnungsrillen - Ø dr	61-0,15		
Schraegstirnrad aussenverzahnt	Berechnungs-Nr. VZB 024 414C vom 28.06.2010		
Zaehnezahl z	32		
Normalmodul m_n	1.50000		mm
Normaleingriffswinkel α_n	17°		
Schraegungswinkel β	32° rechts		
Teilkreisdurchmesser d	56.6006		mm
Grundkreisdurchmesser d_b	53.2481		mm
Steigungshoehe p_z	284.5649		mm
Fusskreisdurchmesser d_f	52.60 ... 52.35		mm
Kopfkreisdurchmesser d_a	61.300 -0.150		mm
Profil-Auswertebereich $L_f...L_a$	5.50 ... 14.02		mm
Nutzkreisdurchmesser $d_{Nf}...d_{Na}$	54.37 ... 60.17		mm
Profil-Winkelabweichung $f_{H\alpha}$	± 0.007		mm
Profil-Formabweichung f_f	0.003		mm
Hoehenballigkeit C_h	0.003 ± 0.002		mm
KopfrueckNahme mit tangentialem	Zug	Schub	
Uebergang C_a	0.008 ±0.004	0.008 ±0.004	mm
- ab Waelzweg L	13.13	13.13	mm
- ab Durchmesser d_{Ca}	59.37	59.37	mm
Rauheit R_z	0.003		mm
Flankenlinien-Auswertebereich L_β	13.60		mm
Flankenlinien-Winkelabweichung $f_{H\beta}$	± 0.011		mm
Flankenlinien-Formabweichung $f_{f\beta}$	0.005		mm
Breitenballigkeit C_b	0.004 ± 0.003		mm
Teilungs-Einzelabweichung f_p	0.005		mm
Teilungs-Spannenabweichung $F_{p\ z/8}$	0.016		mm
Rundlaufabweichung F_r	0.022		mm
Diametrales Zweikugelmass M_e	62.488 ... 62.423		mm
Messkugeldurchmesser D_M	3.000		mm
Fraeserbezugsprofil-Nr.	V03 807 619		
Honradangaben	VZU 023 489		
	Gruenteil gefraest	**nach dem Haerten**	
Zahnweite W	25.809... 25.781	25.812... 25.777	mm
Messzaehnezahl k	6	6	
Diametrales Zweikugelmass M_e	62.791... 62.719	62.800... 62.710	mm
Profil-Winkelabweichung $f_{H\alpha}$	± 0.014	± 0.022	mm
Flankenlinien-Winkelabweichung $f_{H\beta}$	± 0.025	± 0.036	mm
Teilungs-Spannenabweichung $F_{p\ z/8}$	0.040	0.071	mm
Rundlaufabweichung F_r	0.045	0.063	mm
Werkzeug-Bezugsprofil			
Kopfhoehe h_{aP0}	2.630 +0.050		mm
Kopfkantenrundungsradius ρ_{aP0}	0.500 -0.100		mm
Fuss-Formhoehe h_{fP0}	1.280 -0.050 mm		
Kantenbrechflanken-Profilwinkel α_{KP0}	50.00° ±30'		
Protuberanzbetrag pr_{P0}	0.025 ± 0.010 mm		
Protuberanzflanken-Profilwinkel α_{prP0}	10°		
Kopf-Formhoehe h_{FaP0}	(2.11) mm		

Gruenteilwerte sind Richtwerte, die zum Ausgleich von Haerteverzuegen angepasst werden koennen.

11.2. Output gear specification

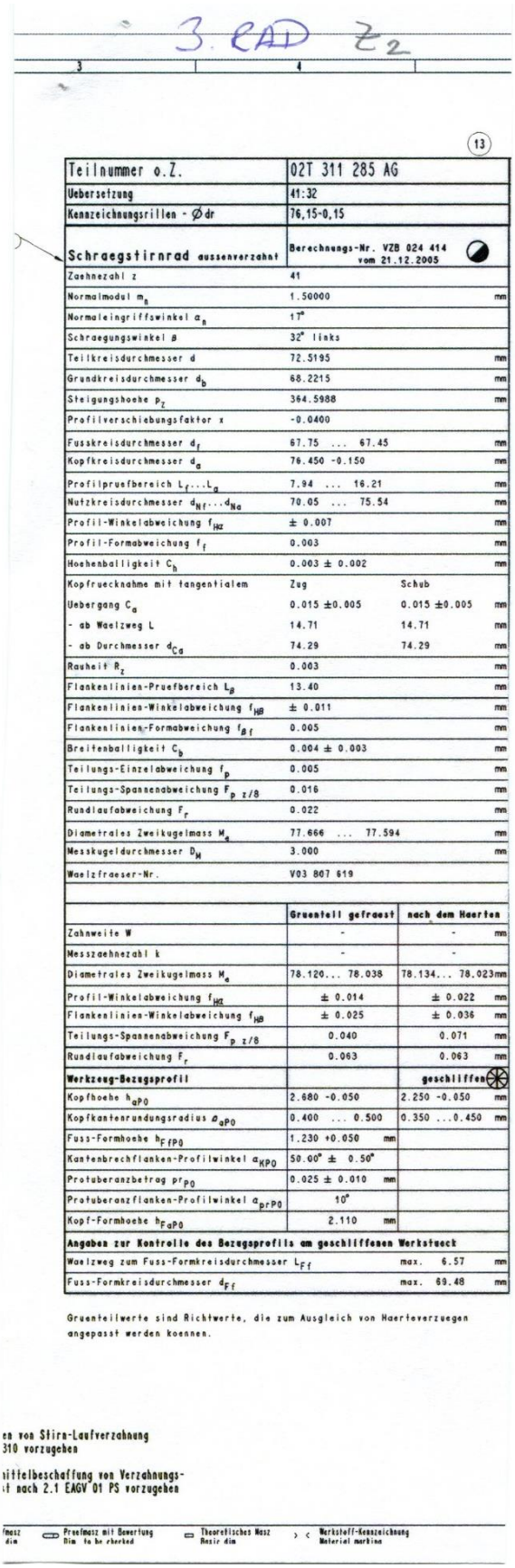

3. CAD z_2

(13)

Teilnummer o.Z.	02T 311 285 AG		
Uebersetzung	41:32		
Kennzeichnungsrillen - Ø dr	76,15-0,15		
Schraegstirnrad aussenverzahnt	Berechnungs-Nr. VZB 024 414 vom 21.12.2005		
Zaehnezahl z	41		
Normalmodul m_n	1.50000		mm
Normaleingriffswinkel α_n	17°		
Schraegungswinkel β	32° links		
Teilkreisdurchmesser d	72.5195		mm
Grundkreisdurchmesser d_b	68.2215		mm
Steigungshoehe p_z	364.5988		mm
Profilverschiebungsfaktor x	-0.0400		
Fusskreisdurchmesser d_f	67.75 ... 67.45		mm
Kopfkreisdurchmesser d_a	76.450 -0.150		mm
Profilpruefbereich $L_f...L_a$	7.94 ... 16.21		mm
Nutzkreisdurchmesser $d_{Nf}...d_{Na}$	70.05 ... 75.54		mm
Profil-Winkelabweichung $f_{H\alpha}$	± 0.007		mm
Profil-Formabweichung f_f	0.003		mm
Hoehenballigkeit C_h	0.003 ± 0.002		mm
Kopfruecknahme mit tangentialem	Zug	Schub	
Uebergang C_a	0.015 ±0.005	0.015 ±0.005	mm
- ab Waelzweg L	14.71	14.71	mm
- ab Durchmesser d_{Ca}	74.29	74.29	mm
Rauheit R_z	0.003		mm
Flankenlinien-Pruefbereich L_β	13.40		mm
Flankenlinien-Winkelabweichung $f_{H\beta}$	± 0.011		mm
Flankenlinien-Formabweichung $f_{f\beta}$	0.005		mm
Breitenballigkeit C_b	0.004 ± 0.003		mm
Teilungs-Einzelabweichung f_p	0.005		mm
Teilungs-Spannenabweichung $F_{p\ z/8}$	0.016		mm
Rundlaufabweichung F_r	0.022		mm
Diametrales Zweikugelmass M_a	77.666 ... 77.594		mm
Messkugeldurchmesser D_M	3.000		mm
Waelzfraeser-Nr.	V03 807 619		

	Gruenteil gefraest	nach dem Haerten	
Zahnweite W	-	-	mm
Messzaehnezahl k	-	-	
Diametrales Zweikugelmass M_a	78.120... 78.038	78.134... 78.023	mm
Profil-Winkelabweichung $f_{H\alpha}$	± 0.014	± 0.022	mm
Flankenlinien-Winkelabweichung $f_{H\beta}$	± 0.025	± 0.036	mm
Teilungs-Spannenabweichung $F_{p\ z/8}$	0.040	0.071	mm
Rundlaufabweichung F_r	0.063	0.063	mm
Werkzeug-Bezugsprofil		geschliffen	
Kopfhoehe h_{aP0}	2.680 -0.050	2.250 -0.050	mm
Kopfkantenrundungsradius ρ_{aP0}	0.400 ... 0.500	0.350 ...0.450	mm
Fuss-Formhoehe h_{fP0}	1.230 +0.050 mm		
Kantenbrechflanken-Profilwinkel α_{KP0}	50.00° ± 0.50°		
Protuberanzbetrag pr_{P0}	0.025 ± 0.010 mm		
Protuberanzflanken-Profilwinkel α_{prP0}	10°		
Kopf-Formhoehe h_{FaP0}	2.110 mm		
Angaben zur Kontrolle des Bezugsprofils am geschliffenen Werkstueck			
Waelzweg zum Fuss-Formkreisdurchmesser L_{Ff}		max. 6.57	mm
Fuss-Formkreisdurchmesser d_{Ff}		max. 69.48	mm

Gruenteilwerte sind Richtwerte, die zum Ausgleich von Haerteverzuegen angepasst werden koennen.

es von Stirn-Laufverzahnung
310 vorzugeben

ittelbeschaffung von Verzahnungs-
t nach 2.1 EAGV 01 PS vorzugeben

fmasz dim | Pruefmasz mit Bewertung Dim to be checked | Theoretisches Masz Basic dim | Werkstoff-Kennzeichnung Material marking